

# On the absence of a universal surface density, and a maximum Newtonian acceleration in dark matter haloes: consequences for MOND

Yong Zhou<sup>a,b</sup>, A. Del Popolo<sup>c,d,e</sup>, Zhe Chang<sup>a,b</sup>

<sup>a</sup>*Institute of High Energy Physics, Chinese Academy of Sciences, Beijing 100049, China*

<sup>b</sup>*School of Physical Sciences, University of Chinese Academy of Sciences, Beijing 100049, China*

<sup>c</sup>*Dipartimento di Fisica e Astronomia, University Of Catania, Via S. Sofia, 64, 95123 Catania, Italy*

<sup>d</sup>*INFN Via S. Sofia, 64, 95125 Catania CT*

<sup>e</sup>*Institute of Astronomy of the Russian Academy of Sciences, Pyatnitskaya Str. 48, 109017 Moscow, Russia*

## Abstract

We study the dark matter (DM) surface density using the SPARC sample and compare it to Donato et al. [1] result. By means of MCMC method, we infer the best-fitting parameters for each galaxy. We reobtain the scaling relation between the surface density and luminosity, and several other scaling laws relating the dark matter halo properties to that of the galactic disc properties. We conclude, in contrast with Donato et al. [1], that the dark matter surface density is not a universal (constant) quantity but correlates with the luminosity as well as with other galactic disc properties. A derived posterior probability distribution of  $\rho_0 r_0$  shows that the null hypothesis of constancy is rejected at a very high confidence level. These results leave little room for the claimed universality of dark matter surface density. Since MOND has strong prediction on the surface density [2], we compared our result with those predictions, finding that MOND predictions are violated by data. To strengthen the previous result, we compared our results to another prediction of MOND [3], the existence of a maximum Newtonian dark matter acceleration in the halo. Also in this case, MOND predictions are in contradiction with data. The dark matter Newtonian acceleration correlates with all the previously presented galactic disc properties, and data are distributed outside the bound predicted by Milgrom & Sanders[3]. We also find that the null hypothesis (constancy of DM Newtonian acceleration) is rejected at a very high confidence level.

## 1. Introduction

The  $\Lambda$  cold dark matter ( $\Lambda$ CDM) model, or concordance cosmology, gives very accurate predictions of the observations on cosmological scales<sup>1</sup> [6–8], and intermediate scales [6–12].

For precision's sake, even at large scale there are tensions of unknown origin between the value of the Hubble parameter,  $H_0$ , and SNe Ia data, the 2013 Planck parameters [13] and  $\sigma_8$  obtained from cluster number counts and weak lensing. Also the Planck 2015 data are in tension with  $\sigma_8$  growth rate [14], and with CFHTLenS weak lensing data [15]. Moreover, a quadrupole-octupole alignment [16–20], a power hemispherical asymmetry [21–26] and a cold spot [27–29] are presented in the large-angle fluctuations in the CMB. Moving to smaller scales ( $\simeq 1 - 10$  kpc), the  $\Lambda$ CDM model is affected by a series of problems [30–42]. Some of them are

- a. the cusp/core (CC) problem [30, 43], that is the discrepancy in the inner profiles obtained in dissipationless N-body simulations [44–46] and observations of dwarf galaxies, Irregulars, and Low Surface Brightness (LSB) galaxies [36, 47–54], and clusters [55];
- b. the “missing satellite problem” (MSP), namely the discrepancy between the number of sub-haloes predicted by N-body simulations [31], and observations;

c. the “Too-Big-To-Fail problem”, namely the fact that sub-haloes are too dense compared to what we observe around the Milky Way [56, 57];

d. the satellites planes problem, that is the difficulty in explaining the location of satellite galaxies of the Milky Way and M31 on planes [58].

Between the solutions proposed, we recall the proposal of modifying the theory of gravity [59–64], modifying the nature of DM [65–68], modifying the power spectrum [69], or delegating the solution to the phenomena related to baryon physics phenomena, which are complex and not well understood. Two of the mechanisms proposed are related to supernovae explosions [70–74], or to transfer of energy and angular momentum from baryons to DM through dynamical friction [36, 49, 53, 75–79].

In order to understand complex phenomena, scaling relations are very helpful.

Kormendy & Freeman [80] found several scaling relations modeling the rotation curves of galaxies through a pseudo-isothermal (pISO) profile. They found several relations between DM halos parameters.

One of those relations, namely  $\rho_0 r_c$ , where  $\rho_0$  is the central density of the density profile, and  $r_c$  is its scale radius, was shown to be independent, in the case of late-type galaxies, from galaxy luminosity. Kormendy & Freeman [80] found that  $\rho_0 r_c \simeq 100 M_\odot pc^{-2}$ .

Email address: adelpopolo@oact.inaf.it (A. Del Popolo)

<sup>1</sup>We recall that at this scales the cosmological constant problem [4, 5], and the cosmic coincidence problem affect the  $\Lambda$ CDM paradigm.

Several other authors went on studying the quoted relation, and in the case of Donato et al. [1] (hereafter D09), the 55 galaxy sample of Kormendy & Freeman [80] was extended by means of  $\simeq 1000$  spiral galaxies, weak lensing of spirals and ellipticals, and data from dwarf galaxies. They found a similar result to that of Kormendy & Freeman [80], which led them to claim a quasi-universality of  $\Sigma_{\text{Donato}}^0 = \rho_0 r_0^2$ , interpreted as central surface density of DM halos. Shortly after the publication of the D09 paper, Milgrom [2] showed that in the Newtonian regime, the modified Newtonian dynamics (MOND) paradigm predicted very similar results to that of D09.

A further extension of the D09 result was that of Gentile et al. [81] (hereafter G09), claiming a quasi-universality of the luminous surface density within scale radius of the dark halo.

A common feature to D09, and G09 is that they used the same sample, and assumed that a very different class of galaxies, going from dwarfs to ellipticals, could be fitted by the same halo density profile, namely the Burkert profile

$$\rho(r) = \frac{\rho_0 r_0^3}{(r + r_0)(r^2 + r_0^2)} \quad (1)$$

obtaining  $\rho_0$ , and  $r_0$ . Now, the Burkert profile is known to give good fits to dwarf galaxies, and LSBs, but not to elliptical galaxies. The DM distribution obtained with different methods (X-ray properties of the emitting hot gas [82, 83], stellar dynamics [84, 85], weak and strong lensing [86, 87]), can be fitted both by the NFW profile or the isothermal profile (a cored profile like the Burkert profile), at least for X-ray data. de Blok et al. [88] found that brighter, larger galaxies with  $M_B > -19$  have density profiles well fitted by both cuspy profiles and cored ones, while less massive galaxies with  $M_B < -19$  are best fitted by cored profiles.

Moreover, even in the case of dwarfs, Simon et al. [89] showed that cored profiles, like Burkert profile, are not a good fit to some of them, and some dSphs could have a cuspy profile [90, 91], instead of a cored one, as expected.

The quoted results bring us at least to have some doubts about the D09, and G09 conclusions, since they are based on the assumption that all the galaxies they studied are well fitted by the Burkert profile, and then they are all cored.

Opposite results to that of D09, and G09 were obtained by Napolitano et al. [92] who showed that the projected density within the local radius is larger in the case of early type galaxies with respect to that of dwarfs and spirals. Boyarsky et al. [93] arrived to similar conclusions with a sample containing group of galaxies, and clusters, much larger than the one of D09, and G09.

They showed that the projected density of local early type galaxies, within the effective radius is larger than that of dwarfs and spirals. This systematic increase with the mass of the halo was also noticed by Boyarsky et al. [93]. The sample of Boyarsky et al. [93] was larger than that of D09, and G09, including groups and clusters. The dark matter column density,

$S$ , defined by them, is increasing with the halo mass as

$$\log_{10} S = 0.21 \log_{10} \frac{M_{\text{halo}}}{10^{10} M_{\odot}} + 1.79 \quad (2)$$

with  $S$  in  $M_{\odot} \text{pc}^{-2}$ . Also Cardone & Tortora [94] showed that the column density and the Newtonian acceleration, obtained through strong lensing, and central velocity dispersion of local galaxies are not constant but correlates, in agreement with Boyarsky et al. [93], with the halo mass  $M_{200}$ , also with the stellar mass  $M_*$ , and the visual luminosity. Napolitano et al. [92] found that the constant density scenario is violated by the early-type galaxies. A correlation of the surface density with  $M_{200}$ , and between the baryon column density and mass, was obtained by Del Popolo et al. [95]. Different from [92], [93] and [94], the result had a smaller scatter. Cardone & Del Popolo [96] followed closely D09, and G09 analysis, doubling the sample of the previous authors, also investigating selection effects, and reobtained the halo parameters fitting all the galaxy, while D09, and G09, for many galaxies obtained from literature. Again they found a result in contradiction to that of D09, and G09, since Newtonian acceleration and virial mass were found to be correlated.

Finally, a more recent result by Li et al. [97], found that fitting the haloes with an Einasto profile, and a DC14 [98] profile the surface density is correlated with luminosity.

We recall that the D09, and especially G09 paper were clearly hinting to a relation of their results with MOND predictions, and was a confirmation of those predictions. This was already confirmed by Milgrom [2]. The results of the previously quoted papers [79, 92–97] showing that the surface density is not a universal quantity, in strong contradiction to D09, and G09, is simply saying that the surface density result contradicts MOND expectation. We will discuss this point in this paper, reobtaining the surface density with the same profile used by D09, and G09, and inferring the parameters through the Markov chain Monte Carlo (MCMC) method. We will also discuss another MOND prediction given by Milgrom & Sanders [3] concerning the existence of a maximum halo acceleration, and using similar methods we show again that data contradicts MOND predictions.

The paper is organized as follows. In Sec. 2, we describe the methodology. In Sec. 3, we analyze the MCMC results and the scaling relations between the dark halo and the galactic disc properties. In Sec. 4, we discuss the impact of our results on MOND. Discussion and conclusions are given in Sec. 5.

## 2. Methodology

### 2.1. SPARC data set

The *Spitzer* Photometry and Accurate Rotation Curves (SPARC) data set<sup>3</sup> [99] is a sample of 175 late-type disc galaxies with new surface photometry at  $3.6 \mu\text{m}$  and high-quality rotation curves from previous HI/H $\alpha$  studies. The surface photometry

---

<sup>2</sup> $\rho_0$  and  $r_0$  are the central density and scale radius of the Burkert profile.

<sup>3</sup><http://astroweb.cwru.edu/SPARC/>

at 3.6  $\mu\text{m}$  provides the stellar mass via the mass-to-light ratio  $\Upsilon_*$  conversion factor. In the near infrared bands,  $\Upsilon_*$  has small changes with star formation history [100, 101], and the distribution of the stellar mass are well determined by *Spitzer* photometry. The 21cm observations provide the gas mass. The majority of SPARC galaxies are characterized by a disc structure, and some have bulges, both of them constitute the stellar component. In total, the galaxy baryonic mass profile includes disc, bulge and gas component and the dark matter profile will be introduced later. In the SPARC data set, the mass profile is represented by velocity at a given radius, so the total baryonic velocity is

$$V_{\text{bar}}^2 = \Upsilon_d V_{\text{disc}}^2 + \Upsilon_b V_{\text{bulge}}^2 + V_{\text{gas}}^2, \quad (3)$$

where  $\Upsilon_d$  and  $\Upsilon_b$  are the mass-to-light ratios for disc and bulge component, respectively. SPARC spans a wide range of morphologies (S0 to Irr), luminosities (5 dex), and surface brightnesses (4 dex). SPARC sample is particularly good to study both DM haloes, and the way they are related to the discs of galaxies.

## 2.2. Dark halo profile

In order to compare our results to that of D09, and G09, in this paper we will use the Burkert profile dark halo to fit the SPARC data set. The choice of this profile is dictated by the fact D09, and G09 used the same profile in their analysis. The Burkert density profile is given by

$$\rho(r) = \frac{\rho_0 r_0^3}{(r + r_0)(r^2 + r_0^2)}, \quad (4)$$

where  $\rho_0$  and  $r_0$  are the central density and scale radius of a halo, respectively. Its enclosed mass profile is given by

$$M(r) = 2\pi\rho_0 r_0^3 [\ln(1+x) + \frac{1}{2} \ln(1+x^2) - \arctan x], \quad (5)$$

where  $x = r/r_0$  is a dimensionless radius. The rotation velocity from DM haloes is given by

$$\frac{V_{\text{DM}}^2}{V_{200}^2} = \frac{C_{200}}{x} \frac{\ln(1+x) + \frac{1}{2} \ln(1+x^2) - \arctan x}{\ln(1+C_{200}) + \frac{1}{2} \ln(1+C_{200}^2) - \arctan C_{200}}. \quad (6)$$

The concentration  $C_{200}$  and the rotation velocity  $V_{200}$  at the virial radius  $r_{200}$  are given by

$$C_{200} = r_{200}/r_0, \quad V_{200} = 10C_{200}r_0H_0, \quad (7)$$

where  $H_0$  is the Hubble constant ( $73 \text{ Km s}^{-1} \text{ Mpc}^{-1}$  in this paper).

The total rotational velocity is given by summing all the components, as

$$V_{\text{tot}}^2 = V_{\text{DM}}^2 + \Upsilon_d V_{\text{disc}}^2 + \Upsilon_b V_{\text{bulge}}^2 + V_{\text{gas}}^2, \quad (8)$$

where  $V_{\text{DM}}$  is the dark matter component, and  $V_{\text{disc}}$ ,  $V_{\text{bulge}}$ ,  $V_{\text{gas}}$  the baryonic component, respectively.  $\Upsilon_d$ , and  $\Upsilon_b$  represent the mass-to-light ratios for the disc and bulge component, which is predicted by the stellar population synthesis model [100, 101]. Apart from the stellar mass-to-light ratios, the galaxy distance

and disc inclination affect the stellar components and the total observed rotational velocities, respectively. If the galaxy distance  $D$  is changed to  $D' = D\delta_D$ , where  $\delta_D$  is a dimensionless distance factor, then the radius changes according to  $R' = R\delta_D$  and the baryonic component velocity changes to  $V'_k = V_k\sqrt{\delta_D}$ , where ‘ $k$ ’ denotes disc, bulge, or gas. If the disc inclination is changed to  $i' = i\delta_i$ , where  $\delta_i$  is a dimensionless inclination factor, the observed rotation curves and its uncertainties change according to

$$V'_{\text{obs}} = V_{\text{obs}} \frac{\sin(i)}{\sin(i')}, \quad \delta V'_{\text{obs}} = \delta V_{\text{obs}} \frac{\sin(i)}{\sin(i')}. \quad (9)$$

Then, we can compare the total rotational velocity with the observed rotation velocity. In total, the free parameters in the fits we will perform are:  $V_{200}$ ,  $C_{200}$ ,  $\Upsilon_d$ ,  $\Upsilon_b$ ,  $\delta_D$  and  $\delta_i$ .

## 2.3. Bayesian analysis

We implement the Bayesian analysis by using the affine-invariant MCMC ensemble sampler in *emcee* [102]. The posterior probability of parameter space is given by

$$P(V_{200}, C_{200}, \Upsilon_d, \Upsilon_b, \delta_D, \delta_i | \text{SPARC}) = \mathcal{L}(V_{200}, C_{200}, \Upsilon_d, \Upsilon_b, \delta_D, \delta_i | \text{SPARC}) P(V_{200}, C_{200}, \Upsilon_d, \Upsilon_b, \delta_D, \delta_i), \quad (10)$$

where the likelihood is derived from the  $\chi^2$  function,  $\mathcal{L} \sim e^{-\chi^2/2}$  and

$$\chi^2 = \sum_{k=1}^N \left( \frac{V_{\text{tot}}(R'_k; V_{200}, C_{200}, \Upsilon_d, \Upsilon_b, \delta_D) - V'_{\text{obs},k}}{\delta V'_{\text{obs},k}} \right)^2, \quad (11)$$

where  $N$  is the number of data point for individual galaxy, the observed rotation curve and its uncertainty at the radius  $R_k$  has been changed to  $V'_{\text{obs},k}$  and  $\delta V'_{\text{obs},k}$ , with a dimensionless factor  $\delta_i$ . The total rotation velocity  $V_{\text{tot}}$  at the radius  $R'_k$  is predicted by the halo parameters  $\{V_{200}, C_{200}\}$  and the galactic parameters  $\{\Upsilon_d, \Upsilon_b, \delta_D\}$ . The prior probability is the product of respective priors,

$$P(V_{200}, C_{200}, \Upsilon_d, \Upsilon_b, \delta_D, \delta_i) = P(V_{200}) P(C_{200}) P(\Upsilon_d) P(\Upsilon_b) P(\delta_D) P(\delta_i). \quad (12)$$

Similarly to Li et al. [97], we impose the same priors on galactic parameters: Gaussian priors on  $\delta_D$  and  $\delta_i$  around 1 with standard deviations given by the observational relative errors; log-normal prior on  $\Upsilon_*$  around their fiducial values  $\Upsilon_d = 0.5$  and  $\Upsilon_b = 0.7$  with a standard deviation of 0.1 dex suggested by the stellar population synthesis models. For halo parameters  $\{V_{200}, C_{200}\}$ , a flat prior is used with  $10 < V_{200} < 500 \text{ km s}^{-1}$ ,  $1 < C_{200} < 100$ . These loose priors have also been used to fit the DC14 and NFW profile in Katz et al. [103]. Moreover, we use flat priors because we want to compare our results with the scaling relations in D09, G09 and Kormendy & Freeman [80, 104] that they obtained by means of flat priors. Finally, the best fitting value is obtained by maximizing the posterior probability.

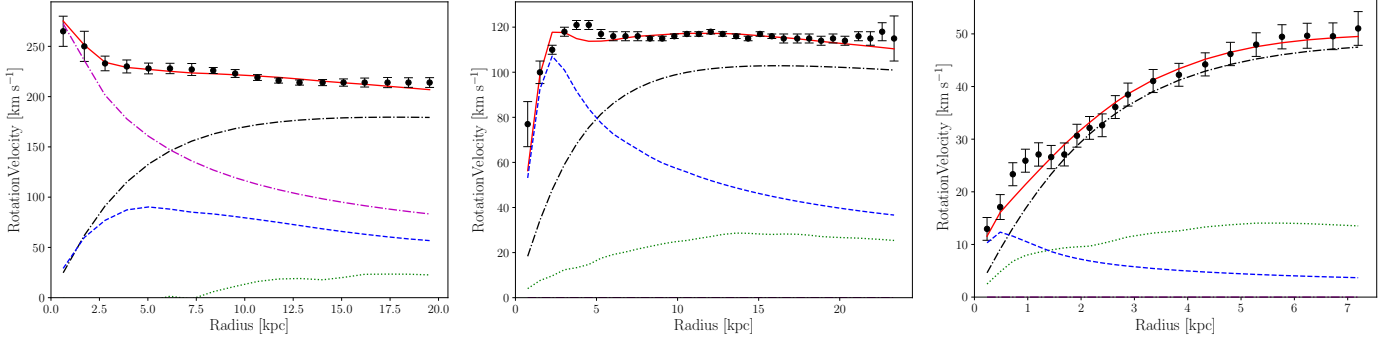


Figure 1: The best fit of galaxy rotation curve for the bulge-dominated spiral galaxy (NGC 7814, left), disc-dominated spiral galaxy (NGC 6503, middle) and gas-dominated dwarf galaxy (NGC 3741, right). The points with error bars show the observed rotation curves. The red line shows the total rotation velocity, the dash-dotted line the dark matter, the dashed line the disc, and the dotted line the gas. Some galaxies have bulge component which is represented by the magenta dash-dotted line.

### 3. Result

#### 3.1. Best fit to individual galaxy

Based on the Bayesian method, we have fit 175 individual galaxy rotation curve in SPARC sample with the Burkert profile. Fig. 1 shows the best fit to three representative galaxies, with the meaning of the symbols described in the caption of the figure. We find that the Burkert profile can give a good fit to the galaxies studied. The reduced  $\chi^2$  for the galaxies in Fig. 1 is 0.867, 2.631, 0.988, respectively.

Except for five galaxies, the galaxies have a reduced  $\chi^2 < 10$ . The best fitting values and the reduced  $\chi^2$  for the full SPARC sample are listed in Table A-1.

In the rest of the paper, we will show the plots obtained using the Burkert profile, since we want to compare our results to that of D09, and G09.

#### 3.2. Correlations between halo and disc properties

In our paper, we studied the correlations between the product of the scale radius,  $r_0$ , and the central density,  $\rho_0$ , with luminosity  $L_{[3.6]}$ . We also showed the correlations between the dark matter acceleration  $g_{\text{DM}}(r_0)$  at scale radius with luminosity  $L_{[3.6]}$ , which will be analyzed later. D09 considered the correlation between  $\rho_0 r_0$ , and the galaxy magnitude,  $M_B$ . Here instead of  $M_B$ , we use  $L_{[3.6]}$ , since in the SPARC sample instead of  $M_B$ , the luminosity  $L_{[3.6]}$  is used. Apart those correlations, we also studied, the correlations between  $\rho_0 r_0$ ,  $g_{\text{DM}}(r_0)$ , and other galaxies disc properties. In the present paper, we are mainly interested in studying the  $\rho_0 r_0$  correlations. This because we want to compare the results with those of D09, and G09. As we already reported, D09, and G09 claimed a quasi-universality of  $\rho_0 r_0$ , where  $r_0$  are the scale radius for the Burkert profile, and  $\rho_0$  the central density. G09 extended the result to baryons, claiming that the D09 result was valid for luminous matter surface density. In the following, we will show that fitting SPARC data by means of the Burkert profile like that used by D09, and G09, we do not find any quasi-universal relation, in agreement with several papers in literature [79, 92–97].

All the figures in this paper shows the quantity  $\rho_0 r_0$  on the left vertical axis, and  $g_{\text{DM}}(r_0)$  on the right vertical axis in order to reduce the number of figures. This can be done since  $\rho_0 r_0$ , and  $g_{\text{DM}}(r_0)$  are proportional as shown in the next sections.

In Fig. 2, we show the scaling relation between  $\rho_0 r_0$  and  $L_{[3.6]}$ , when imposing flat priors on the halo parameters. Errors on  $\rho_0 r_0$ , were obtained by error propagation based on the uncertainties in the fitting parameters, while the uncertainty on  $L_{[3.6]}$  are obtained from SPARC dataset, and is given by the quadratic sum of errors on distances and flux. The blue line in Fig 2 denotes the linear regression in log-space. The horizontal dashed line and the gray shaded region represent the predictions of D09 concerning the surface density, namely  $\log_{10} \rho_0 r_0 = 2.15 \pm 0.2$  in units of  $M_\odot \text{pc}^{-2}$ . The correlation strength is evaluated through the Pearson correlation coefficient  $R$  and the  $p$ -value. The second one is the probability that the real data is reproduced by an uncorrelated system. Since the  $p$ -value is small, we convert it to the number of  $\sigma$  from zero,  $n = \sqrt{2} \text{erf}^{-1}(1 - p)$ , where  $\text{erf}^{-1}$  is the inverse error function. Then the significance level for correlation is  $n\sigma$ . In this scaling relation,  $R = 0.33$ , and we find that the significance level for correlation is  $4.45\sigma$ , indicating a medium correlation between the two variables. This result is shown in Table 1. The smaller value of the Pearson coefficient  $R$  in our case with respect to Li et al. [97] is due to the flat prior on halo parameters we used. It seems that Gaussian priors used in Li et al. [97] impose a strong constraints on the halo parameters. We fit the data by using the linear regression and we find a linear relation in log-space,

$$\log_{10} \rho_0 r_0 = (0.13 \pm 0.02) \log_{10} L_{[3.6]} + (0.95 \pm 0.23). \quad (13)$$

The quoted result is in contradiction to that of D09, G09, and Kormendy & Freeman [80, 104], which does not show any correlation (flat line). The dark halo profile we used for our fit is the same of that of D09, and G09, while Kormendy & Freeman [104] used a non-singular isothermal sphere. In the present paper, we are interested in a comparison with D09, so we are not going to consider the changes due to non-singular isothermal sphere, that however should be small since the Burkert profile, excluding the outer regions, has a similar behavior to the non-

Table 1: The linear regression between the dark halo surface density and the galactic disc properties. (1) – the linear regression equation; (2) – the Pearson correlation coefficient  $R$ ; (3) – the significance level<sup>\*</sup>.

Equation (1)	$R$ (2)	$n\sigma$ (3)
$\log_{10} \rho_0 r_0 = (0.13 \pm 0.02) \log_{10} L_{[3.6]} + (0.95 \pm 0.23)$	0.33	$4.45\sigma$
$\log_{10} \rho_0 r_0 = -(0.07 \pm 0.01)T + (2.72 \pm 0.07)$	-0.42	$5.81\sigma$
$\log_{10} \rho_0 r_0 = (0.90 \pm 0.12) \log_{10} V_{\text{flat}} + (0.42 \pm 0.25)$	0.54	$6.81\sigma$
$\log_{10} \rho_0 r_0 = (0.46 \pm 0.08) \log_{10} R_{\text{eff}} + (2.08 \pm 0.04)$	0.15	$1.94\sigma$
$\log_{10} \rho_0 r_0 = (0.25 \pm 0.04) \log_{10} \Sigma_{\text{eff}} + (1.73 \pm 0.09)$	0.50	$7.07\sigma$
$\log_{10} \rho_0 r_0 = (0.32 \pm 0.08) \log_{10} R_{\text{disc}} + (2.17 \pm 0.04)$	0.14	$1.88\sigma$
$\log_{10} \rho_0 r_0 = (0.36 \pm 0.04) \log_{10} \Sigma_{\text{disc}} + (1.27 \pm 0.11)$	0.51	$7.21\sigma$
$\log_{10} \rho_0 r_0 = (0.32 \pm 0.08) \log_{10} R_{\text{HI}} + (1.90 \pm 0.10)$	0.14	$1.84\sigma$
$\log_{10} \rho_0 r_0 = (0.22 \pm 0.04) \log_{10} M_{\text{HI}} + (0.20 \pm 0.39)$	0.20	$2.67\sigma$

<sup>\*</sup>  $n = \sqrt{2} \operatorname{erf}^{-1}(1 - p)$ , where  $p$ -value is the probability that the real data is reproduced by an uncorrelated system.

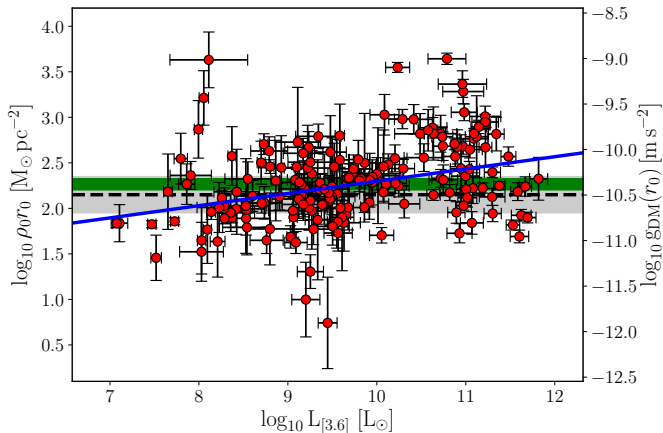


Figure 2: Scaling relations between the  $\rho_0 r_0$  (left vertical axis),  $g_{\text{DM}}(r_0)$  (right vertical axis), and  $L_{[3.6]}$  for the Burkert profile when imposing flat prior on the halo parameters. The dashed black line, and the gray shaded region, represent the value  $\log_{10} \rho_0 r_0 = 2.15 \pm 0.2$  obtained by D09. The blue line denotes the linear regression in log-space. The green shaded region, represents the range  $0.3a_0 - 0.4a_0$  for the maximum halo acceleration predicted by Milgrom & Sanders [3].

singular isothermal sphere.

As we already discussed, we used the Burkert profile in order our analysis is similar to that of D09. A comparison of our result, Fig. 2, with their result shows they do not agree. While D09 do not find any correlation between  $\rho_0 r_0$  and magnitude (luminosity), in our case there is a correlation similarly to previously cited papers [79, 92–97].

So summarizing, following the method used by D09, we found a result contradicting theirs. Apart the correlation, Fig. 2 shows that our data are not contained in the D09 range, showing again that D09 result is not in agreement with ours: there is no hint of a quasi-universal behavior of  $\rho_0 r_0$ , and this conclusion is again in agreement with several papers [79, 92–96].

We want to add that D09 analysis has some issues. As noticed by Li et al. [97], in D09 stellar contributions is taken into

account using several methods and adopting spectro-photometric galaxy models. Thus, the contributions of each component strongly depend on the efficacy of the modeling. Moreover, for several galaxies, D09 did not fit the rotation curve using the Burkert profile but relied on values already presented in literature, and based on different dark halo profiles. We improved the previous issues by fitting each SPARC galaxy rotation curve to obtain the Burkert parameters, using the MCMC method, also to infer a realistic estimate of the errors on the quantities of interest.

The analysis in Spino et al. [105] and Kormendy & Freeman [104] also shows some inappropriate choices. As noticed by Li et al. [97], and previously reported by D09, the use of the maximum disc analysis by Kormendy & Freeman [80, 104] produces drawbacks, as pushing  $\Upsilon_{\text{disc}}$  to unreasonably high values in the case of low mass galaxies. Spino et al. [105] assumed constant  $\Upsilon_*$ , while in the optical band a strong variation of  $\Upsilon_*$  is expected [100].

### 3.3. Other correlations

In order to show that the correlation we find is a genuine one, we looked for other correlations between  $\rho_0 r_0$  and the galaxy disc properties as tabulated in the SPARC data set [99]. The result of the analysis is plotted in Fig. 3. The first correlation we found is with galaxy type, characterized by  $R = -0.42$ , having a significance level of  $5.81\sigma$ , and

$$\log_{10} \rho_0 r_0 = -(0.07 \pm 0.01)T + (2.72 \pm 0.07). \quad (14)$$

It shows that earlier galaxies have a larger surface density.

The second one is with the rotation velocity along the flat part (only 135 galaxies have the flat part),  $V_{\text{flat}}$ , characterized by  $R = 0.54$ , indicating a strong correlation with a significance level of  $6.81\sigma$ , and

$$\log_{10} \rho_0 r_0 = (0.90 \pm 0.12) \log_{10} V_{\text{flat}} + (0.42 \pm 0.25). \quad (15)$$

We also found that there exist strong correlations with the baryonic surface brightness, which can be converted into surface density via the mass-to-light ratio. Also the effective surface brightness,  $\Sigma_{\text{eff}}$ , and the central surface brightness of the

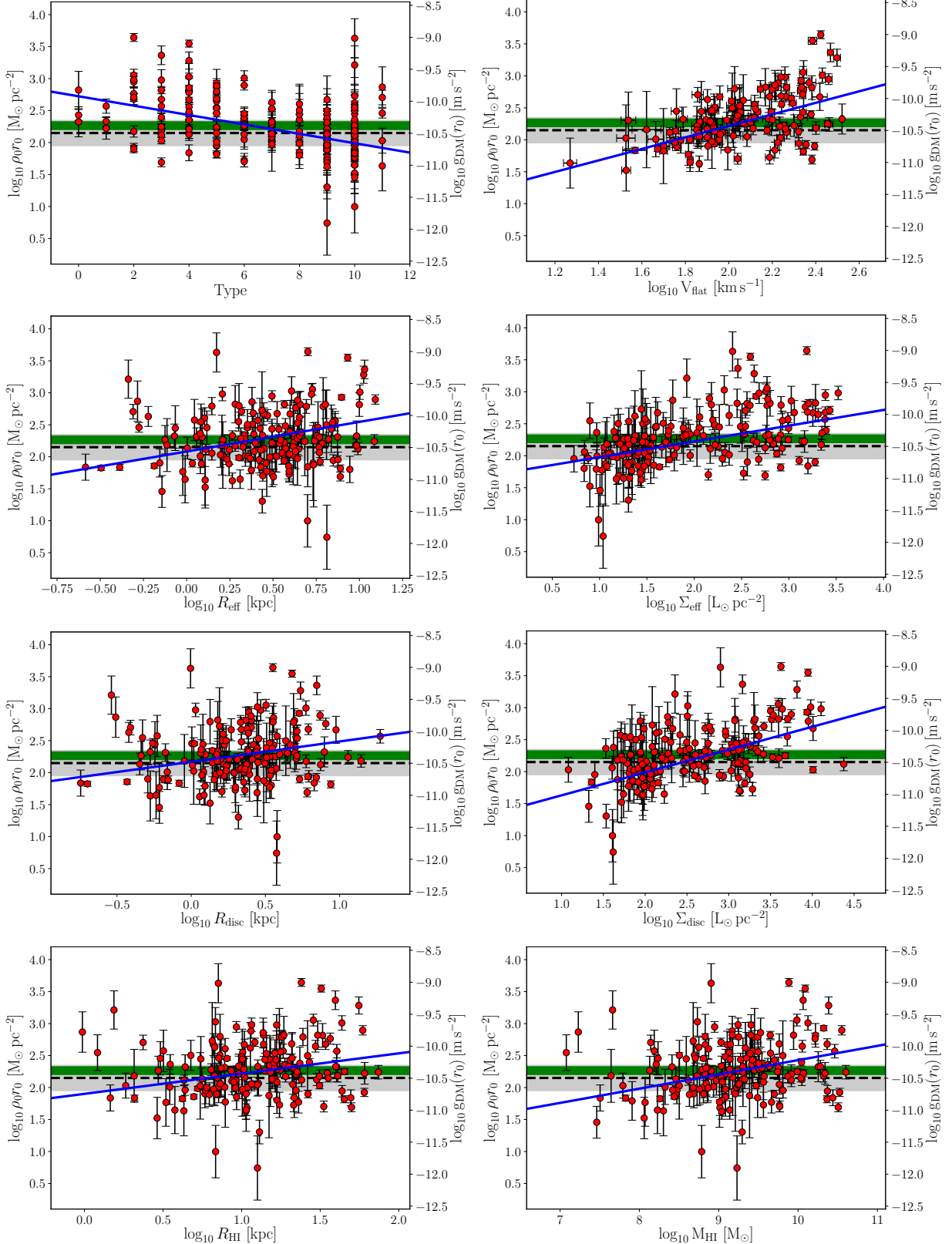


Figure 3: Scaling relations between the  $\rho_0 r_0$  (left vertical axis),  $g_{\text{DM}}(r_0)$  (right vertical axis) vs galactic properties. The blue line denotes the linear regression in log-space (except the Hubble type). The dashed black line, and the gray shaded region, represent the value  $\log_{10} \rho_0 r_0 = 2.15 \pm 0.2$  obtained by D09. The green shaded region, represents the range  $0.3a_0 - 0.4a_0$  for the maximum halo acceleration predicted by Milgrom & Sanders [3]. Circles with error bars correspond to the data obtained by means of the SPARC sample. The panels show the correlations: 1.  $\rho_0 r_0(\text{GDM})$  – numerical Hubble type; 2.  $\rho_0 r_0(\text{GDM})$  – rotation velocity along the flat part; 3.  $\rho_0 r_0(\text{GDM})$  – effective radius; 4.  $\rho_0 r_0(\text{GDM})$  – effective surface brightness; 5.  $\rho_0 r_0(\text{GDM})$  – scale length of the stellar disc; 6.  $\rho_0 r_0(\text{GDM})$  – central surface brightness of the stellar disc; 7.  $\rho_0 r_0(\text{GDM})$  – HI radius; 8.  $\rho_0 r_0(\text{GDM})$  – total HI mass.

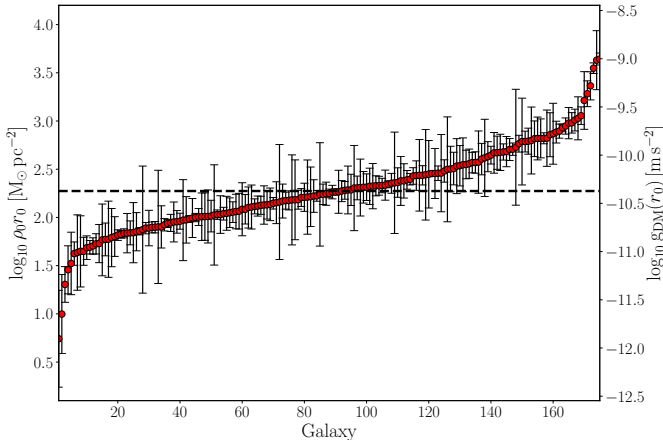


Figure 4: The derived posterior probability distributions of  $\rho_0 r_0$  (left vertical axis) and  $g_{\text{DM}}(r_0)$  (right vertical axis) for 175 SPARC galaxies. The red circles show the maximum of the posterior in ascending order. The error bars show its uncertainties. The global best-fit value of  $\rho_0 r_0$ ,  $g_{\text{DM}}(r_0)$  is shown by the dashed line.

stellar disc,  $\Sigma_{\text{disc}}$  can be expressed in terms of the dark halo surface density, strongly correlated to  $\rho_0 r_0$ . There still exist positive correlations with the effective radius,  $R_{\text{eff}}$ , and the scale length of the stellar disc,  $R_{\text{disc}}$ , but the correlations are weak. We also find other two correlations with the total mass of atomic hydrogen (HI),  $M_{\text{HI}}$ , and with the radius where the HI surface density reaches  $1 \text{ M}_\odot \text{ pc}^{-2}$ . These results are summarized in Table 1.

In all panels, the horizontal dashed line and the gray shaded band represent the predictions of D09 concerning the surface density, namely  $\log_{10} \rho_0 r_0 = 2.15 \pm 0.2 \text{ M}_\odot \text{ pc}^{-2}$ .

Summarizing, in our analysis we followed closely D09 analysis, and differently from them we found a correlation between  $\rho_0 r_0$  and luminosity, in agreement with several previous studies [79, 92–97]. Moreover, our data do not fulfill the D09 claim that  $\log_{10} \rho_0 r_0 = 2.15 \pm 0.2 \text{ M}_\odot \text{ pc}^{-2}$ .

The main point of the previous plots is that the quoted correlations leave small room to the idea that  $\rho_0 r_0$  is constant.

In order to have a more quantitative idea, following Rodrigues et al. [64], we calculated the confidence level to reject the hypothesis of a constant value of  $\rho_0 r_0$ . Fig. 4 show the derived posterior probability distributions of  $\rho_0 r_0$  for 175 SPARC galaxies. Each red circle shows the maximum of the posterior, and the dashed line is the global best-fit of  $\rho_0 r_0$ . We find that the global best-fit value is  $\log_{10} \rho_0 r_0 = 2.27$ , i.e.,  $\rho_0 r_0 = 187.94 \text{ M}_\odot \text{ pc}^{-2}$ . Most of galaxies are quite incompatible with the global best-fit. The null hypothesis (constancy of the  $\rho_0 r_0$ ) is rejected at  $> 10\sigma$ . After excluding low-quality galaxies following the quality criteria in Rodrigues et al. [64], namely using the same 100 galaxies, we find that the null hypothesis is still rejected at  $> 10\sigma$ .

#### 4. The surface density, DM Newtonian acceleration and MOND

As several times reported, D09 found that the product  $\Sigma_{\text{Donato}}^0 = \rho_0 r_0$ , dubbed surface density, is constant, independent on  $M_B$  magnitude (i.e., luminosity), in a very large magnitude range:  $-8 \geq M_B \geq -22$ , having the value,

$$\log_{10} \frac{\Sigma_{\text{Donato}}^0}{\text{M}_\odot \text{ pc}^{-2}} = 2.15 \pm 0.2. \quad (16)$$

From Eq. 16, one gets the gravitational acceleration coming from the dark matter component at the scale radius

$$g_{\text{dark}}(r_0) = G\pi\Sigma_{\text{dark}}(r_0) = 3.2^{+1.8}_{-1.2} 10^{-9} \text{ cm s}^{-2}, \quad (17)$$

where  $\Sigma_{\text{dark}}(r_0) = 0.51\Sigma_{\text{Donato}}^0$  is the dark matter mean surface density within the scale radius  $r_0$ . This acceleration assumes always the same value.

G09 extended this result to the luminous component in galaxies,

$$g_{\text{bary}}(r_0) = G\pi\Sigma_{\text{bary}}(r_0), \quad (18)$$

where  $\Sigma_{\text{bary}}(r_0)$  is the baryonic mean surface density within  $r_0$  and they found  $g_{\text{bary}}(r_0) = 5.7^{+3.8}_{-2.8} 10^{-10} \text{ cm s}^{-2}$ .

This implies that a. the gravitational acceleration coming from the DM component, and the luminous galaxies component at the scale radius ( $r_0$ ) the luminous-to-dark matter ratio, is constant; b. in a scale radius ( $r_0$ ) the luminous-to-dark matter ratio, is constant; c. the central baryonic surface density correlates with the core radius. The quoted claims were interpreted as a “correlation” between the enclosed surface densities of luminous and dark matter in galaxies. Another interpretation that was given is that the DM halo core radius is the radius beyond which  $g_{\text{bary}}(r) < 6 \times 10^{-10} \text{ cm s}^{-2}$ , relating the result to the so called mass discrepancy-acceleration relation [61]. From the “universal and maximum” acceleration  $g_{\text{dark}}(r_0)$ , the mass discrepancy-acceleration relation predicts, by definition, the existence of a universal gravity coming from baryons at  $r_0$ , and a universal surface density in  $r_0$ .

In other words, there is a strict correlation between the constancy (universality) of the surface density and a universal acceleration, that is nothing else than the well known universal acceleration in MOND,  $a_0$ .

Milgrom [2] prompted by the previous results showed that MOND predicts, for all object having a mean acceleration at or above  $a_0$ , a quasi-universal central surface density of galaxy DM haloes, which can be written as

$$\Sigma_{\text{MOND}}^0 = \gamma \Sigma_M = \gamma \frac{a_0}{2\pi G}, \quad (19)$$

where  $0.7 < \gamma < 2$ , for the limiting form of the interpolating function used in [2], and

$$\Sigma_M = 138 \frac{a_0}{1.2 \times 10^{-8} \text{ cm s}^{-2}} \text{ M}_\odot \text{ pc}^{-2}, \quad (20)$$

that for a canonical value of  $a_0$  gives  $\Sigma_M = 138 \text{ M}_\odot \text{ pc}^{-2}$ , or  $\log_{10} \frac{\Sigma_M}{\text{M}_\odot \text{ pc}^{-2}} = 2.14$ , in agreement with Eq. (16). In the case of

low surface density systems, having accelerations smaller than  $a_0$ ,  $\Sigma_{\text{MOND}}^0 \simeq 2.4(\Sigma_b^0 \Sigma_M)^{1/2} \simeq (6/\pi + 1)\Sigma_M X_0 \simeq 0.6\Sigma_M$ , being  $X_0 \simeq 0.2$ , and  $\Sigma_b^0$  the central baryon surface density. The previous result was generalized by [106], in  $\Sigma_{\text{MOND}}^0 = \Sigma_M S(\Sigma_b^0/\Sigma_M)$ , where the function  $S(y) = \int_0^y v(y') dy'$ , and  $v$  is the interpolating function. In summary, Milgrom [2] confirms D09 result, adding that the quasi-universal value is not shared by objects with low surface densities, and that values lower than  $\Sigma_{\text{Donato}}^0$  are allowed in low surface density systems. To be conservative, D09 result together with Milgrom [2] can be written as

$$1.9 < \log_{10} \Sigma_{\text{MOND}}^0 < 2.4, \quad (21)$$

which almost coincide with the range  $1.95 < \log_{10} \Sigma_{\text{Donato}}^0 < 2.35$  [1]. Moreover, Eq. (19) with Eq. (21) impose a limit on  $a_0$ , showing that there is a strict correlation between the surface density properties and MOND.

A spontaneous question, at this point is: are our data on  $\Sigma_{\text{Donato}}^0 = \rho_0 r_0$  compatible with MOND predictions?

As shown in Fig. 2, the relation between  $\Sigma_{\text{Donato}}^0 = \rho_0 r_0$  and the luminosity is not flat as predicted in D09, but show a precise correlation already discussed. The plot also shows that the distribution of the points in Fig. 2 is largely outside the prediction of D09. Fig. 3, shows a similar behavior. The relations between  $\rho_0 r_0$  and the quantities in the x-axis, are never flat, and the points are largely distributed out from the D09 boundaries. Moreover, the condition Eq. (21), is violated by our data, implying that Milgrom [2] prediction obtained by means of MOND is violated by data, and this is a big problem for MOND.

We can do another check using another MOND prediction given by Milgrom & Sanders [3] concerning the existence of a maximum halo acceleration. This results comes out from the relation

$$g_h(g) = g - g_N = g - g\mu(g/a_0) \quad (22)$$

where  $g$  is the true MOND acceleration,  $g_h$  the halo acceleration,  $g_N$  the Newtonian acceleration, and  $\mu$  is MOND interpolation function.  $g_h$  cannot exceed  $a_{\text{max}} = \eta a_0$ , with  $\eta \simeq 0.3 - 0.4$  according to the standard interpolation function,  $\mu(x) = \frac{x}{\sqrt{1+x^2}}$ .

We calculated, from the plot of the correlation between the surface density and luminosity, Fig. 2 (left axis <sup>4</sup>), the correlation between the acceleration and the luminosity, that we plotted in Fig. 2 (right axis). From Fig. 2 (right axis), it can be seen that our data do not confirm MOND prediction. In Fig. 3 (right axis), we also show the DM Newtonian acceleration vs galactic properties, showing the halo maximum accelerations predicted by MOND. Following Milgrom & Sanders [3], we plot the band  $0.3a_0 \sim 0.4a_0$  (green area), indicating the range in which the maximum halo acceleration can be. Some of the galaxies have values of  $g_{\text{DM}}(r_0)$  that are not only higher than  $0.4a_0$  but even  $a_0$ .

The previous conclusion is strengthened by Fig. 3 (right axis) showing that  $g_{\text{DM}}(r_0)$  is correlated with several quantities of the galactic disc, and again the plots show that the data violates the MOND [3] predictions.

Moreover, we follow the method introduced in Rodrigues et al. [64] to calculate the confidence level to reject a constant value of  $g_{\text{DM}}(r_0)$ . Fig. 4 (right axis) show the derived posterior probability distributions of  $g_{\text{DM}}(r_0)$  for 175 SPARC galaxies. We find that the global best-fit value is  $\log_{10} g_{\text{DM}}(r_0) = -10.37$ , i.e.,  $g_{\text{DM}}(r_0) = 0.42 \times 10^{-10} \text{ m s}^{-2}$ . Note that even if the global best-fit of  $g_{\text{DM}}(r_0)$  is  $0.35a_0$ , in the MOND prediction range  $0.3a_0 \sim 0.4a_0$ , for most of galaxies,  $g_{\text{DM}}(r_0)$  is incompatible with the global best-fit. The null hypothesis (constancy of the  $g_{\text{DM}}(r_0)$ ) is rejected at  $> 10\sigma$ . Even if we exclude those galaxies with low-quality following the quality criteria in Rodrigues et al. [64] and use the same 100 galaxies, we find that the null hypothesis is still rejected at  $> 10\sigma$ .

## 5. Discussion and Conclusions

In this paper, using SPARC sample, we verified the D09 claim of the existence of a universal surface density of dark matter haloes. We calculated the  $\rho_0 r_0$  for the Burkert profile, by using the MCMC method. We looked for correlations between the quoted quantity and luminosity, as done by D09, and also we verified if our  $\rho_0 r_0$  data satisfied D09 result, namely  $\log_{10} \rho_0 r_0 = 2.15 \pm 0.2 \text{ M}_\odot \text{ pc}^{-2}$ . We repeated the calculation, looking for correlation with a series of other disc properties (Hubble type, rotation velocity along the flat part, effective radius, effective surface brightness, scale length of the stellar disc, central surface brightness of the stellar disc, total HI mass and HI radius), finding similar results to that of the  $\rho_0 r_0 - L_{[3,6]}$  correlation. The calculations, performed through Bayesian statistics, showed that contrarily to D09 conclusions, that the surface density is not a universal quantity. As shown by Milgrom [2], MOND has a strong prediction for the surface density. We verified if our data is consistent with that prediction, but we found the opposite result. To strengthen the previous result, we used another of the predictions of MOND [3], related to the existence of a maximum value for halo Newtonian acceleration,  $g_{\text{DM}}(r_0)$ , predicted to be in the range  $0.3a_0 \sim 0.4a_0$  for the standard interpolation function. Also in this case, MOND predictions are in contradiction with data. The dark matter Newtonian acceleration correlates with all the previously presented galactic properties, and our calculated  $g_{\text{DM}}(r_0)$  is outside the boundary predicted by MOND. We also calculated the confidence level to reject a constancy of  $g_{\text{DM}}(r_0)$  and we find that the null hypothesis is rejected at a very high confidence level.

The present paper is related to Rodrigues' [64]. Like us, they use the SPARC database to show that the probability to have a fundamental acceleration (e.g., the typical MOND acceleration,  $a_0$ ), is practically 0, and that  $a_0$  must be of emergent nature. The analysis in the present paper, leads us to a similar conclusion. In this paper, we were not interested in studying what is the origin of the emergent nature of  $a_0$ . This was studied by a recent paper (Grudic et al. 2019, arXiv:1910.06345), which in agreement with our paper and [64], concludes that the

<sup>4</sup>We write left axis to refer to  $\rho_0 r_0$ , and right axis to refer to  $g_{\text{DM}}(r_0)$ .

origin of the quoted acceleration is emergent rather than fundamental. Moreover, according to their study, the acceleration comes naturally from stellar feedback.

We may conclude that our results show the absence of a universal surface density, and the absence of maximum acceleration in haloes. Since these quantities are related to MOND, which has precise predictions for them, rejected by a comparison with data, this imply that MOND shows big problems at small scales, the scales at which should give its best.

## Acknowledgments

We are thankful for the open access of the SPARC data set. ZC is supported by the National Natural Science Fund of China under grant Nos. 11675182 and 11690022.

## References

- [1] F. Donato, G. Gentile, P. Salucci, C. Frigerio Martins, M. I. Wilkinson, G. Gilmore, E. K. Grebel, A. Koch, R. Wyse, A constant dark matter halo surface density in galaxies, *MNRAS*397 (2009) 1169–1176. [arXiv:0904.4054](#), doi:10.1111/j.1365-2966.2009.15004.x.
- [2] M. Milgrom, The central surface density of ‘dark haloes’ predicted by MOND, *MNRAS*398 (2009) 1023–1026. [arXiv:0909.5184](#), doi:10.1111/j.1365-2966.2009.15255.x.
- [3] M. Milgrom, R. H. Sanders, MOND predictions of ‘halo’ phenomenology in disc galaxies, *MNRAS*357 (2005) 45–48. [arXiv:astro-ph/0406487](#), doi:10.1111/j.1365-2966.2004.08578.x.
- [4] S. Weinberg, The cosmological constant problem, *Reviews of Modern Physics* 61 (1989) 1–23. doi:10.1103/RevModPhys.61.1.
- [5] A. V. Astashenok, A. del Popolo, Cosmological measure with volume averaging and the vacuum energy problem, *Classical and Quantum Gravity* 29 (8) (2012) 085014. [arXiv:1203.2290](#), doi:10.1088/0264-9381/29/8/085014.
- [6] E. Komatsu, K. M. Smith, J. Dunkley, C. L. Bennett, B. Gold, G. Hinshaw, N. Jarosik, D. Larson, M. R. Nolta, L. Page, Seven-year Wilkinson Microwave Anisotropy Probe (WMAP) Observations: Cosmological Interpretation, *ApJS*192 (2) (2011) 18. [arXiv:1001.4538](#), doi:10.1088/0067-0049/192/2/18.
- [7] A. Del Popolo, Dark matter, density perturbations, and structure formation, *Astronomy Reports* 51 (3) (2007) 169–196. [arXiv:0801.1091](#), doi:10.1134/S1063772907030018.
- [8] A. Del Popolo, Non-baryonic dark matter in cosmology 1548 (2013) 2–63. doi:10.1063/1.4817029.
- [9] D. N. Spergel, L. Verde, H. V. Peiris, E. Komatsu, M. R. Nolta, C. L. Bennett, M. Halpern, G. Hinshaw, N. Jarosik, A. Kogut, M. Limon, S. S. Meyer, L. Page, G. S. Tucker, J. L. Weiland, E. Wollack, E. L. Wright, First-Year Wilkinson Microwave Anisotropy Probe (WMAP) Observations: Determination of Cosmological Parameters, *ApJS*148 (2003) 175–194. [arXiv:astro-ph/0302209](#), doi:10.1086/377226.
- [10] M. Kowalski, D. Rubin, G. Aldering, R. J. Agostinho, A. Amadon, R. Amanullah, C. Balland, K. Barbary, G. Blanc, P. J. Challis, A. Connoley, e. a. Connolly, N. V., Improved Cosmological Constraints from New, Old, and Combined Supernova Data Sets, *ApJ*686 (2008) 749–778. [arXiv:0804.4142](#), doi:10.1086/589937.
- [11] W. J. Percival, B. A. Reid, D. J. Eisenstein, N. A. Bahcall, T. Budavari, J. A. Frieman, M. Fukugita, J. E. Gunn, e. a. Ivezić, Ž., Baryon acoustic oscillations in the Sloan Digital Sky Survey Data Release 7 galaxy sample, *MNRAS*401 (2010) 2148–2168. [arXiv:0907.1660](#), doi:10.1111/j.1365-2966.2009.15812.x.
- [12] A. Del Popolo, Nonbaryonic Dark Matter in Cosmology, *International Journal of Modern Physics D* 23 (2014) 30005. [arXiv:1305.0456](#), doi:10.1142/S0218271814300055.
- [13] Planck Collaboration, P. A. R. Ade, N. Aghanim, C. Armitage-Caplan, M. Arnaud, M. Ashdown, F. Atrio-Barandela, J. Aumont, C. Baccigalupi, A. J. Banday, et al., Planck 2013 results. XVI. Cosmological parameters, *A&A*571 (2014) A16. [arXiv:1303.5076](#), doi:10.1051/0004-6361/201321591.
- [14] E. Macaulay, I. K. Wehus, H. K. Eriksen, Lower Growth Rate from Recent Redshift Space Distortion Measurements than Expected from Planck, *Physical Review Letters* 111 (16) (2013) 161301. [arXiv:1303.6583](#), doi:10.1103/PhysRevLett.111.161301.
- [15] M. Raveri, Is there concordance within the concordance  $\Lambda$ CDM model?, *ArXiv e-prints* (Oct. 2015). [arXiv:1510.00688](#).
- [16] D. J. Schwarz, G. D. Starkman, D. Huterer, C. J. Copi, Is the Low- $l$  Microwave Background Cosmic?, *Physical Review Letters* 93 (22) (2004) 221301. [arXiv:astro-ph/0403353](#), doi:10.1103/PhysRevLett.93.221301.
- [17] C. J. Copi, D. Huterer, D. J. Schwarz, G. D. Starkman, On the large-angle anomalies of the microwave sky, *MNRAS*367 (2006) 79–102. [arXiv:astro-ph/0508047](#), doi:10.1111/j.1365-2966.2005.09980.x.
- [18] C. J. Copi, D. Huterer, D. J. Schwarz, G. D. Starkman, Uncorrelated universe: Statistical anisotropy and the vanishing angular correlation function in WMAP years 1–3, *Phys. Rev. D*75 (2) (2007) 023507. [arXiv:astro-ph/0605135](#), doi:10.1103/PhysRevD.75.023507.
- [19] C. J. Copi, D. Huterer, D. J. Schwarz, G. D. Starkman, Large-Angle Anomalies in the CMB, *Advances in Astronomy* 2010 (2010) 847541. [arXiv:1004.5602](#), doi:10.1155/2010/847541.
- [20] C. J. Copi, D. Huterer, D. J. Schwarz, G. D. Starkman, Large-scale alignments from WMAP and Planck, *MNRAS*449 (2015) 3458–3470. [arXiv:1311.4562](#), doi:10.1093/mnras/stv501.
- [21] H. K. Eriksen, F. K. Hansen, A. J. Banday, K. M. Górski, P. B. Lilje, Asymmetries in the Cosmic Microwave Background Anisotropy Field, *ApJ*605 (2004) 14–20. [arXiv:astro-ph/0307507](#), doi:10.1086/382267.
- [22] F. K. Hansen, A. J. Banday, K. M. Górski, Testing the cosmological principle of isotropy: local power-spectrum estimates of the WMAP data, *MNRAS*354 (2004) 641–665. [arXiv:astro-ph/0404206](#), doi:10.1111/j.1365-2966.2004.08229.x.
- [23] T. R. Jaffe, A. J. Banday, H. K. Eriksen, K. M. Górski, F. K. Hansen, Evidence of Vorticity and Shear at Large Angular Scales in the WMAP Data: A Violation of Cosmological Isotropy?, *ApJ*629 (2005) L1–L4. [arXiv:astro-ph/0503213](#), doi:10.1086/444454.
- [24] J. Hoftuft, H. K. Eriksen, A. J. Banday, K. M. Górski, F. K. Hansen, P. B. Lilje, Increasing Evidence for Hemispherical Power Asymmetry in the Five-Year WMAP Data, *ApJ*699 (2009) 985–989. [arXiv:0903.1229](#), doi:10.1088/0004-637X/699/2/985.
- [25] Planck Collaboration, P. A. R. Ade, N. Aghanim, C. Armitage-Caplan, M. Arnaud, M. Ashdown, F. Atrio-Barandela, J. Aumont, C. Baccigalupi, A. J. Banday, et al., Planck 2013 results. XXIII. Isotropy and statistics of the CMB, *A&A*571 (2014) A23. [arXiv:1303.5083](#), doi:10.1051/0004-6361/201321534.
- [26] Y. Akrami, Y. Faintye, A. Shafieloo, H. K. Eriksen, F. K. Hansen, A. J. Banday, K. M. Górski, Power Asymmetry in WMAP and Planck Temperature Sky Maps as Measured by a Local Variance Estimator, *ApJ*784 (2014) L42. [arXiv:1402.0870](#), doi:10.1088/2041-8205/784/2/L42.
- [27] M. Cruz, E. Martínez-González, P. Vielva, L. Cayón, Detection of a non-Gaussian spot in WMAP, *MNRAS*356 (2005) 29–40. [arXiv:astro-ph/0405341](#), doi:10.1111/j.1365-2966.2004.08419.x.
- [28] M. Cruz, M. Tucci, E. Martínez-González, P. Vielva, The non-Gaussian cold spot in WilkinsonMicrowaveAnisotropyProbe: significance, morphology and foreground contribution, *MNRAS*369 (2006) 57–67. [arXiv:astro-ph/0601427](#), doi:10.1111/j.1365-2966.2006.10312.x.
- [29] M. Cruz, L. Cayón, E. Martínez-González, P. Vielva, J. Jin, The Non-Gaussian Cold Spot in the 3 Year Wilkinson Microwave Anisotropy Probe Data, *ApJ*655 (2007) 11–20. [arXiv:astro-ph/0603859](#), doi:10.1086/509703.
- [30] B. Moore, Evidence against dissipation-less dark matter from observations of galaxy haloes, *Nature*370 (1994) 629–631. doi:10.1038/370629a0.
- [31] B. Moore, T. Quinn, F. Governato, J. Stadel, G. Lake, Cold collapse and the core catastrophe, *MNRAS*310 (1999) 1147–1152. [arXiv:astro-ph/9903164](#), doi:10.1046/j.1365-8711.1999.03039.x.
- [32] J. P. Ostriker, P. Steinhardt, New Light on Dark Matter, *Science*

- 300 (2003) 1909–1914. [arXiv:astro-ph/0306402](#), doi:10.1126/science.1085976.
- [33] M. Boylan-Kolchin, J. S. Bullock, M. Kaplinghat, Too big to fail? The puzzling darkness of massive Milky Way subhaloes, *MNRAS*415 (2011) L40–L44. [arXiv:1103.0007](#), doi:10.1111/j.1745-3933.2011.01074.x.
- [34] M. Boylan-Kolchin, J. S. Bullock, M. Kaplinghat, The Milky Way’s bright satellites as an apparent failure of  $\Lambda$ CDM, *MNRAS*422 (2012) 1203–1218. [arXiv:1111.2048](#), doi:10.1111/j.1365-2966.2012.20695.x.
- [35] S.-H. Oh, C. Brook, F. Governato, E. Brinks, L. Mayer, W. J. G. de Blok, A. Brooks, F. Walter, The Central Slope of Dark Matter Cores in Dwarf Galaxies: Simulations versus THINGS, *AJ*142 (2011) 24. [arXiv:1011.2777](#), doi:10.1088/0004-6256/142/1/24.
- [36] A. Del Popolo, N. Hiotelis, Cusps and cores in the presence of galactic bulges, *J. Cosmology Astropart. Phys.*1 (2014) 47. [arXiv:1401.6577](#), doi:10.1088/1475-7516/2014/01/047.
- [37] A. Del Popolo, M. Le Delliou, A unified solution to the small scale problems of the  $\Lambda$ CDM model II: introducing parent-satellite interaction, *J. Cosmology Astropart. Phys.*2014 (12) (2014) 051. [arXiv:1408.4893](#), doi:10.1088/1475-7516/2014/12/051.
- [38] A. Del Popolo, F. Pace, The Cusp/Core problem: supernovae feedback versus the baryonic clumps and dynamical friction model, *Ap&SS*361 (5) (2016) 162. [arXiv:1502.01947](#), doi:10.1007/s10509-016-2742-z.
- [39] A. Del Popolo, M. Le Delliou, Small Scale Problems of the  $\Lambda$ CDM Model: A Short Review, *Galaxies*5 (1) (2017) 17. [arXiv:1606.07790](#), doi:10.3390/galaxies5010017.
- [40] Y. Zhou, Z.-C. Zhao, Z. Chang, Searching for a cosmological preferred direction with 147 rotationally supported galaxies, *Astrophys. J.*847 (2) (2017) 86. [arXiv:1707.00417](#), doi:10.3847/1538-4357/aa8991.
- [41] Z. Chang, H.-N. Lin, Z.-C. Zhao, Y. Zhou, Searching for a possible dipole anisotropy in acceleration scale with 147 rotationally supported galaxies, *Chin. Phys. C42* (11) (2018) 115103. [arXiv:1803.08344](#), doi:10.1088/1674-1137/42/11/115103.
- [42] Z. Chang, Y. Zhou, Is there a fundamental acceleration scale in galaxies?, *MNRAS*486 (2) (2019) 1658–1666. [arXiv:1812.05002](#), doi:10.1093/mnras/stz961.
- [43] R. A. Flores, J. R. Primack, Observational and theoretical constraints on singular dark matter halos, *ApJ*427 (1994) L1–L4. [arXiv:astro-ph/9402004](#), doi:10.1086/187350.
- [44] J. F. Navarro, C. S. Frenk, S. D. M. White, The Structure of Cold Dark Matter Halos, *ApJ*462 (1996) 563. [arXiv:astro-ph/9508025](#), doi:10.1086/177173.
- [45] J. F. Navarro, C. S. Frenk, S. D. M. White, A Universal Density Profile from Hierarchical Clustering, *ApJ*490 (1997) 493. [arXiv:astro-ph/9611107](#), doi:10.1086/304888.
- [46] J. F. Navarro, A. Ludlow, V. Springel, J. Wang, M. Vogelsberger, S. D. M. White, A. Jenkins, C. S. Frenk, A. Helmi, The diversity and similarity of simulated cold dark matter haloes, *MNRAS*402 (2010) 21–34. [arXiv:0810.1522](#), doi:10.1111/j.1365-2966.2009.15878.x.
- [47] W. J. G. de Blok, A. Bosma, S. McGaugh, Simulating observations of dark matter dominated galaxies: towards the optimal halo profile, *MNRAS*340 (2003) 657–678. [arXiv:astro-ph/0212102](#), doi:10.1046/j.1365-8711.2003.06330.x.
- [48] R. A. Swaters, B. F. Madore, F. C. van den Bosch, M. Balcells, The Central Mass Distribution in Dwarf and Low Surface Brightness Galaxies, *ApJ*583 (2003) 732–751. [arXiv:astro-ph/0210152](#), doi:10.1086/345426.
- [49] A. Del Popolo, The Cusp/Core Problem and the Secondary Infall Model, *ApJ*698 (2009) 2093–2113. [arXiv:0906.4447](#), doi:10.1088/0004-637X/698/2/2093.
- [50] A. Del Popolo, P. Kroupa, Density profiles of dark matter haloes on galactic and cluster scales, *A&A*502 (2009) 733–747. [arXiv:0906.1146](#), doi:10.1051/0004-6361/200811404.
- [51] S.-H. Oh, W. J. G. de Blok, E. Brinks, F. Walter, R. C. Kennicutt, Jr., Dark and Luminous Matter in THINGS Dwarf Galaxies, *AJ*141 (2011) 193. [arXiv:1011.0899](#), doi:10.1088/0004-6256/141/6/193.
- [52] R. Kuzio de Naray, T. Kaufmann, Recovering cores and cusps in dark matter haloes using mock velocity field observations, *MNRAS*414 (2011) 3617–3626. [arXiv:1012.3471](#), doi:10.1111/j.1365-2966.2011.18656.x.
- [53] A. Del Popolo, Density profile slopes of dwarf galaxies and their environment, *MNRAS*419 (2012) 971–984. [arXiv:1105.0090](#), doi:10.1111/j.1365-2966.2011.19754.x.
- [54] A. Del Popolo, On the density-profile slope of clusters of galaxies, *MNRAS*424 (2012) 38–51. [arXiv:1204.4439](#), doi:10.1111/j.1365-2966.2012.21141.x.
- [55] A. Del Popolo, The flat density profiles of massive, and relaxed galaxy clusters, *J. Cosmology Astropart. Phys.*2014 (7) (2014) 019. [arXiv:1407.4347](#), doi:10.1088/1475-7516/2014/07/019.
- [56] S. Garrison-Kimmel, M. Rocha, M. Boylan-Kolchin, J. S. Bullock, J. Lally, Can feedback solve the too-big-to-fail problem?, *MNRAS*433 (2013) 3539–3546. [arXiv:1301.3137](#), doi:10.1093/mnras/stt984.
- [57] S. Garrison-Kimmel, M. Boylan-Kolchin, J. S. Bullock, E. N. Kirby, Too big to fail in the Local Group, *MNRAS*444 (2014) 222–236. [arXiv:1404.5313](#), doi:10.1093/mnras/stu1477.
- [58] M. S. Pawłowski, B. Famaey, H. Jerjen, D. Merritt, P. Kroupa, J. Dabringhausen, F. Lüghausen, D. A. Forbes, G. Hensler, F. Hammer, M. Puech, S. Fouquet, H. Flores, Y. Yang, Co-orbiting satellite galaxy structures are still in conflict with the distribution of primordial dwarf galaxies, *MNRAS*442 (2014) 2362–2380. [arXiv:1406.1799](#), doi:10.1093/mnras/stu1005.
- [59] H. A. Buchdahl, Non-linear Lagrangians and cosmological theory, *MNRAS*150 (1970) 1.
- [60] A. A. Starobinsky, A new type of isotropic cosmological models without singularity, *Physics Letters B* 91 (1980) 99–102. doi:10.1016/0370-2693(80)90670-X.
- [61] M. Milgrom, A modification of the Newtonian dynamics as a possible alternative to the hidden mass hypothesis, *ApJ*270 (1983) 365–370. doi:10.1086/161130.
- [62] M. Milgrom, A modification of the Newtonian dynamics - Implications for galaxies, *ApJ*270 (1983) 371–389. doi:10.1086/161131.
- [63] R. Ferraro, f(R) and f(T) theories of modified gravity 1471 (2012) 103–110. [arXiv:1204.6273](#), doi:10.1063/1.4756821.
- [64] D. C. Rodrigues, V. Marra, A. del Popolo, Z. Davari, Absence of a fundamental acceleration scale in galaxies, *Nat. Astron.*2 (8) (2018) 668–672. [arXiv:1806.06803](#), doi:10.1038/s41550-018-0498-9.
- [65] P. Colín, V. Avila-Reese, O. Valenzuela, Substructure and Halo Density Profiles in a Warm Dark Matter Cosmology, *ApJ*542 (2000) 622–630. [arXiv:astro-ph/0004115](#), doi:10.1086/317057.
- [66] J. Goodman, Repulsive dark matter, *New A5* (2000) 103–107. [arXiv:astro-ph/0003018](#), doi:10.1016/S1384-1076(00)00015-4.
- [67] P. J. E. Peebles, Fluid Dark Matter, *ApJ*534 (2000) L127–L129. [arXiv:astro-ph/0002495](#), doi:10.1086/312677.
- [68] J. Sommer-Larsen, A. Dolgov, Formation of Disk Galaxies: Warm Dark Matter and the Angular Momentum Problem, *ApJ*551 (2001) 608–623. [arXiv:astro-ph/9912166](#), doi:10.1086/320211.
- [69] A. R. Zentner, J. S. Bullock, Halo Substructure and the Power Spectrum, *ApJ*598 (2003) 49–72. [arXiv:astro-ph/0304292](#), doi:10.1086/378797.
- [70] J. F. Navarro, V. R. Eke, C. S. Frenk, The cores of dwarf galaxy haloes, *MNRAS*283 (1996) L72–L78. [arXiv:astro-ph/9610187](#).
- [71] S. Gelato, J. Sommer-Larsen, On DDO 154 and cold dark matter halo profiles, *MNRAS*303 (1999) 321–328. [arXiv:astro-ph/9806289](#), doi:10.1046/j.1365-8711.1999.02223.x.
- [72] J. I. Read, G. Gilmore, Mass loss from dwarf spheroidal galaxies: the origins of shallow dark matter cores and exponential surface brightness profiles, *MNRAS*356 (2005) 107–124. [arXiv:astro-ph/0409565](#), doi:10.1111/j.1365-2966.2004.08424.x.
- [73] S. Mashchenko, H. M. P. Couchman, J. Wadsley, The removal of cusps from galaxy centres by stellar feedback in the early Universe, *Nature*442 (2006) 539–542. [arXiv:astro-ph/0605672](#), doi:10.1038/nature04944.
- [74] F. Governato, C. Brook, L. Mayer, A. Brooks, G. Rhee, J. Wadsley, P. Jonsson, B. Willman, G. Stinson, T. Quinn, P. Madau, Bulgeless dwarf galaxies and dark matter cores from supernova-driven outflows, *Nature*463 (2010) 203–206. [arXiv:0911.2237](#), doi:10.1038/nature08640.
- [75] A. El-Zant, I. Shlosman, Y. Hoffman, Dark Halos: The Flattening of the

- Density Cusp by Dynamical Friction, ApJ560 (2001) 636–643. arXiv: astro-ph/0103386, doi:10.1086/322516.
- [76] A. A. El-Zant, Y. Hoffman, J. Primack, F. Combes, I. Shlosman, Flatcored Dark Matter in Cuspy Clusters of Galaxies, ApJ607 (2004) L75–L78. arXiv:astro-ph/0309412, doi:10.1086/421938.
- [77] E. Romano-Díaz, I. Shlosman, Y. Hoffman, C. Heller, Erasing Dark Matter Cusps in Cosmological Galactic Halos with Baryons, ApJ685 (2008) L105–L108. arXiv:0808.0195, doi:10.1086/592687.
- [78] D. R. Cole, W. Dehnen, M. I. Wilkinson, Weakening dark matter cusps by clumpy baryonic infall, MNRAS416 (2011) 1118–1134. arXiv: 1105.4050, doi:10.1111/j.1365-2966.2011.19110.x.
- [79] A. Saburova, A. Del Popolo, On the surface density of dark matter haloes, MNRAS445 (2014) 3512–3524. arXiv:1410.3052, doi:10.1093/mnras/stu1957.
- [80] J. Kormendy, K. C. Freeman, Scaling Laws for Dark Matter Halos in Late-Type and Dwarf Spheroidal Galaxies 220 (2004) 377. arXiv: astro-ph/0407321.
- [81] G. Gentile, B. Famaey, H. Zhao, P. Salucci, Universality of galactic surface densities within one dark halo scale-length, Nature461 (2009) 627–628. arXiv:0909.5203, doi:10.1038/nature08437.
- [82] R. Nagino, K. Matsushita, Gravitational potential and X-ray luminosities of early-type galaxies observed with XMM-Newton and Chandra, A&A501 (2009) 157–169. arXiv:0903.2540, doi:10.1051/0004–6361/200810978.
- [83] D. A. Buote, P. J. Humphrey, Dark Matter in Elliptical Galaxies, in: D.-W. Kim, S. Pellegrini (Eds.), Astrophysics and Space Science Library, Vol. 378 of Astrophysics and Space Science Library, 2012, p. 235. arXiv:1104.0012, doi:10.1007/978-1-4614-0580-1\_8.
- [84] O. Gerhard, Dark Matter and Elliptical Galaxy Dynamics, Highlights of Astronomy 15 (2010) 65–65. doi:10.1017/S1743921310008203.
- [85] N. R. Napolitano, A. J. Romanowsky, M. Capaccioli, N. G. Douglas, M. Arnaboldi, L. Coccato, O. Gerhard, K. Kuijken, M. R. Merrifield, S. P. Bamford, A. Cortesi, P. Das, K. C. Freeman, The PN.S Elliptical Galaxy Survey: a standard  $\Lambda$ CDM halo around NGC 4374?, MNRAS411 (2011) 2035–2053. arXiv:1010.1533, doi:10.1111/j.1365–2966.2010.17833.x.
- [86] J. An, H. Zhao, Fitting functions for dark matter density profiles, MNRAS428 (4) (2013) 2805–2811. arXiv:1209.6220, doi:10.1093/mnras/sts175.
- [87] N. Lyskova, E. Churazov, T. Naab, Mass density slope of elliptical galaxies from strong lensing and resolved stellar kinematics, MNRAS475 (2) (2018) 2403–2414. arXiv:1711.01123, doi:10.1093/mnras/sty018.
- [88] W. J. G. de Blok, F. Walter, E. Brinks, C. Trachternach, S.-H. Oh, R. C. Kennicutt, Jr., High-Resolution Rotation Curves and Galaxy Mass Models from THINGS, AJ136 (2008) 2648–2719. arXiv:0810.2100, doi:10.1088/0004–6256/136/6/2648.
- [89] J. D. Simon, A. D. Bolatto, A. Leroy, L. Blitz, E. L. Gates, High-Resolution Measurements of the Halos of Four Dark Matter-Dominated Galaxies: Deviations from a Universal Density Profile, ApJ621 (2005) 757–776. arXiv:astro-ph/0412035, doi:10.1086/427684.
- [90] L. E. Strigari, C. S. Frenk, S. D. M. White, Kinematics of Milky Way satellites in a Lambda cold dark matter universe, MNRAS408 (2010) 2364–2372. arXiv:1003.4268, doi:10.1111/j.1365–2966.2010.17287.x.
- [91] M. A. Breddels, A. Helmi, Model comparison of the dark matter profiles of Fornax, Sculptor, Carina and Sextans, A&A558 (2013) A35. arXiv: 1304.2976, doi:10.1051/0004–6361/201321606.
- [92] N. R. Napolitano, A. J. Romanowsky, C. Tortora, The central dark matter content of early-type galaxies: scaling relations and connections with star formation histories, MNRAS405 (2010) 2351–2371. arXiv: 1003.1716, doi:10.1111/j.1365–2966.2010.16710.x.
- [93] A. Boyarsky, O. Ruchayskiy, D. Iakubovskyi, A. V. Maccio', D. Malyshev, New evidence for dark matter, ArXiv e-prints (Nov. 2009). arXiv: 0911.1774.
- [94] V. F. Cardone, C. Tortora, Dark matter scaling relations in intermediate z haloes, MNRAS409 (2010) 1570–1576. arXiv:1007.3673, doi:10.1111/j.1365–2966.2010.17398.x.
- [95] A. Del Popolo, V. F. Cardone, G. Belvedere, Surface density of dark matter haloes on galactic and cluster scales, MNRAS429 (2013) 1080–1087. arXiv:1212.6797, doi:10.1093/mnras/sts389.
- [96] V. F. Cardone, A. Del Popolo, Newtonian acceleration scales in spiral galaxies, MNRAS427 (2012) 3176–3187. arXiv:1209.1524, doi:10.1111/j.1365–2966.2012.21982.x.
- [97] P. Li, F. Lelli, S. S. McGaugh, N. Starkman, J. M. Schombert, A constant characteristic volume density of dark matter haloes from SPARC rotation curve fits, Mon. Not. Roy. Astron. Soc. 482 (4) (2019) 5106–5124. arXiv:1811.00553, doi:10.1093/mnras/sty2968.
- [98] A. Di Cintio, C. B. Brook, A. A. Dutton, A. V. Maccio, G. S. Stinson, A. Knebe, A mass-dependent density profile for dark matter haloes including the influence of galaxy formation, MNRAS441 (4) (2014) 2986–2995. arXiv:1404.5959, doi:10.1093/mnras/stu729.
- [99] F. Lelli, S. S. McGaugh, J. M. Schombert, SPARC: Mass Models for 175 Disk Galaxies with Spitzer Photometry and Accurate Rotation Curves, Astron. J. 152 (2016) 157. arXiv:1606.09251, doi:10.3847/0004–6256/152/6/157.
- [100] S. S. McGaugh, J. M. Schombert, Color-Mass-to-light-ratio Relations for Disk Galaxies, AJ148 (2014) 77. arXiv:1407.1839, doi:10.1088/0004–6256/148/5/77.
- [101] S. E. Meidt, E. Schinnerer, G. van de Ven, D. Zaritsky, R. Peletier, J. H. Knapen, K. Sheth, M. Regan, M. Querejeta, J.-C. Muñoz-Mateos, Reconstructing the Stellar Mass Distributions of Galaxies Using S<sup>4</sup>G IRAC 3.6 and 4.5  $\mu$ m Images. II. The Conversion from Light to Mass, ApJ788 (2) (2014) 144. arXiv:1402.5210, doi:10.1088/0004–637X/788/2/144.
- [102] D. Foreman-Mackey, D. W. Hogg, D. Lang, J. Goodman, emcee: The MCMC Hammer, PASP125 (2013) 306. arXiv:1202.3665, doi:10.1086/670067.
- [103] H. Katz, F. Lelli, S. S. McGaugh, A. Di Cintio, C. B. Brook, J. M. Schombert, Testing feedback-modified dark matter haloes with galaxy rotation curves: estimation of halo parameters and consistency with  $\Lambda$ CDM scaling relations, MNRAS466 (2) (2017) 1648–1668. arXiv: 1605.05971, doi:10.1093/mnras/stw3101.
- [104] J. Kormendy, K. C. Freeman, Scaling Laws for Dark Matter Halos in Late-type and Dwarf Spheroidal Galaxies, ApJ817 (2016) 84. arXiv: 1411.2170, doi:10.3847/0004–637X/817/2/84.
- [105] M. Spano, M. Marcellin, P. Amram, C. Carignan, B. Epinat, O. Hernandez, GHASP: an H $\alpha$  kinematic survey of spiral and irregular galaxies - V. Dark matter distribution in 36 nearby spiral galaxies, MNRAS383 (2008) 297–316. arXiv:0710.1345, doi:10.1111/j.1365–2966.2007.12545.x.
- [106] M. Milgrom, Universal Modified Newtonian Dynamics Relation between the Baryonic and “Dynamical” Central Surface Densities of Disc Galaxies, Physical Review Letters 117 (14) (2016) 141101. arXiv: 1607.05103, doi:10.1103/PhysRevLett.117.141101.

**A. The best fitting value for full SPARC sample**

Table A-1: The best-fitting values of galactic parameters and dark halo parameters for the Burkert profile with flat prior. These galaxies are sorted by luminosity. The scale radius  $r_0$ , central density  $\rho_0$ , and its product  $\rho_0 r_0$  are deduced from the best-fitting values of halo parameters. The reduced  $\chi^2$  for those galaxies whose data points more than the fitting parameters are listed in the last column.

SPARC ID	Galaxy Name	$\delta_D$	$\delta_i$	$\Upsilon_d$	$\Upsilon_b$	$\log_{10} V_{200}$ ( $\text{km s}^{-2}$ )	$\log_{10} C_{200}$	$\log_{10} r_0$ (kpc)	$\log_{10} \rho_0$ ( $\text{M}_\odot \text{pc}^{-3}$ )	$\log_{10} \rho_0 r_0$ ( $\text{M}_\odot \text{pc}^{-2}$ )	$\chi^2_r$
001	UGC02487	1.16 ± 0.14	1.20 ± 0.12	0.68 ± 0.14	0.69 ± 0.14	2.26 ± 0.04	1.10 ± 0.14	1.30 ± 0.14	-1.98 ± 0.37	2.33 ± 0.23	4.807
002	UGC02885	1.08 ± 0.09	1.02 ± 0.06	0.57 ± 0.11	0.97 ± 0.11	2.32 ± 0.03	1.00 ± 0.09	1.46 ± 0.11	-2.22 ± 0.21	2.24 ± 0.11	1.097
003	NGC6195	0.99 ± 0.09	0.99 ± 0.07	0.40 ± 0.08	0.78 ± 0.09	2.24 ± 0.10	1.01 ± 0.11	1.36 ± 0.20	-2.18 ± 0.27	2.18 ± 0.10	1.789
004	UGC11455	0.67 ± 0.13	1.00 ± 0.01	0.32 ± 0.06	.....	2.17 ± 0.02	1.59 ± 0.08	0.71 ± 0.10	-0.71 ± 0.21	3.01 ± 0.11	1.699
005	NGC5371	0.76 ± 0.13	1.01 ± 0.04	0.86 ± 0.13	.....	2.69 ± 0.05	0.63 ± 0.07	2.19 ± 0.09	-3.06 ± 0.15	2.13 ± 0.09	10.263
006	NGC2955	0.97 ± 0.09	0.92 ± 0.10	0.33 ± 0.06	0.94 ± 0.15	2.20 ± 0.04	1.30 ± 0.06	1.04 ± 0.07	-1.47 ± 0.16	2.57 ± 0.11	3.731
007	NGC0801	1.04 ± 0.09	1.00 ± 0.01	0.63 ± 0.06	.....	2.22 ± 0.05	0.76 ± 0.07	1.60 ± 0.11	-2.79 ± 0.15	1.82 ± 0.06	8.122
008	ESO563-G021	0.55 ± 0.14	0.99 ± 0.04	0.30 ± 0.07	.....	2.22 ± 0.03	1.72 ± 0.10	0.64 ± 0.12	-0.35 ± 0.26	3.28 ± 0.13	8.771
009	UGC09133	1.22 ± 0.15	1.07 ± 0.09	0.73 ± 0.10	0.40 ± 0.05	2.22 ± 0.02	0.84 ± 0.05	1.51 ± 0.06	-2.59 ± 0.11	1.92 ± 0.06	7.886
010	UGC02953	0.49 ± 0.12	0.94 ± 0.07	0.14 ± 0.02	1.63 ± 0.20	2.11 ± 0.04	1.99 ± 0.05	0.25 ± 0.08	0.39 ± 0.13	3.64 ± 0.06	7.952
011	NGC7331	0.89 ± 0.09	1.00 ± 0.03	0.47 ± 0.06	0.58 ± 0.13	2.19 ± 0.02	1.19 ± 0.05	1.14 ± 0.06	-1.75 ± 0.12	2.40 ± 0.06	1.287
012	NGC3992	0.98 ± 0.10	1.00 ± 0.04	0.45 ± 0.13	.....	2.15 ± 0.05	1.48 ± 0.15	0.80 ± 0.19	-0.99 ± 0.37	2.82 ± 0.18	1.400
013	NGC6674	1.37 ± 0.16	1.15 ± 0.09	0.85 ± 0.15	0.73 ± 0.16	2.41 ± 0.05	0.48 ± 0.08	2.06 ± 0.11	-3.37 ± 0.15	1.69 ± 0.07	1.440
014	NGC5985	0.66 ± 0.21	0.99 ± 0.03	0.30 ± 0.06	0.81 ± 0.21	2.14 ± 0.03	1.81 ± 0.10	0.47 ± 0.13	-0.10 ± 0.28	3.37 ± 0.15	2.990
015	NGC2841	1.13 ± 0.08	1.07 ± 0.07	1.08 ± 0.10	0.85 ± 0.09	2.30 ± 0.01	1.02 ± 0.04	1.42 ± 0.05	-2.17 ± 0.09	2.25 ± 0.04	1.810
016	IC4202	0.31 ± 0.05	1.00 ± 0.01	0.37 ± 0.07	0.20 ± 0.03	2.00 ± 0.01	2.00 ± 0.04	0.14 ± 0.05	0.41 ± 0.11	3.55 ± 0.06	4.646
017	NGC5005	0.96 ± 0.08	1.00 ± 0.03	0.50 ± 0.09	0.59 ± 0.09	2.08 ± 0.24	1.44 ± 0.20	0.78 ± 0.41	-1.11 ± 0.51	2.67 ± 0.21	0.099
018	NGC5907	0.98 ± 0.05	1.00 ± 0.02	0.19 ± 0.03	.....	2.10 ± 0.01	1.58 ± 0.03	0.66 ± 0.03	-0.73 ± 0.07	2.93 ± 0.04	8.533
019	UGC05253	0.85 ± 0.15	0.96 ± 0.09	0.35 ± 0.07	0.93 ± 0.16	2.14 ± 0.04	1.45 ± 0.06	0.82 ± 0.08	-1.06 ± 0.15	2.77 ± 0.09	0.956
020	NGC5055	1.01 ± 0.03	1.10 ± 0.09	0.38 ± 0.04	.....	2.06 ± 0.02	1.16 ± 0.03	1.03 ± 0.02	-1.81 ± 0.07	2.22 ± 0.06	2.202
021	NGC2998	1.15 ± 0.13	1.01 ± 0.03	0.72 ± 0.09	.....	2.16 ± 0.04	0.90 ± 0.08	1.40 ± 0.12	-2.45 ± 0.20	1.94 ± 0.09	4.002
022	UGC11914	1.05 ± 0.18	1.13 ± 0.10	0.45 ± 0.07	0.78 ± 0.13	2.70 ± 0.07	1.22 ± 0.05	1.62 ± 0.10	-1.67 ± 0.13	2.95 ± 0.08	0.588
023	NGC3953	0.97 ± 0.14	1.00 ± 0.02	0.47 ± 0.14	.....	1.96 ± 0.25	1.58 ± 0.37	0.52 ± 0.55	-0.73 ± 0.90	2.79 ± 0.45	0.438
024	UGC12506	1.00 ± 0.10	1.00 ± 0.04	0.42 ± 0.09	.....	2.13 ± 0.01	1.54 ± 0.05	0.73 ± 0.06	-0.84 ± 0.13	2.90 ± 0.07	0.796
025	NGC0891	0.94 ± 0.05	1.00 ± 0.01	0.24 ± 0.03	0.62 ± 0.07	2.04 ± 0.01	1.55 ± 0.04	0.63 ± 0.05	-0.81 ± 0.10	2.82 ± 0.06	2.032
026	UGC06614	0.98 ± 0.10	0.93 ± 0.13	0.50 ± 0.12	0.69 ± 0.15	2.23 ± 0.05	1.05 ± 0.11	1.31 ± 0.12	-2.09 ± 0.27	2.22 ± 0.17	0.095
027	UGC02916	0.87 ± 0.12	0.92 ± 0.09	0.47 ± 0.11	0.70 ± 0.11	2.10 ± 0.04	1.42 ± 0.05	0.82 ± 0.06	-1.14 ± 0.13	2.68 ± 0.08	10.545
028	UGC03205	0.92 ± 0.15	1.00 ± 0.06	0.15 ± 0.03	0.85 ± 0.17	2.06 ± 0.02	1.68 ± 0.06	0.51 ± 0.08	-0.46 ± 0.17	3.06 ± 0.09	4.358
029	NGC5033	1.00 ± 0.16	1.00 ± 0.01	0.45 ± 0.09	0.51 ± 0.10	2.09 ± 0.01	1.41 ± 0.07	0.81 ± 0.08	-1.17 ± 0.17	2.65 ± 0.09	2.509
030	NGC4088	0.97 ± 0.12	1.00 ± 0.03	0.46 ± 0.07	.....	2.46 ± 0.22	0.88 ± 0.14	1.72 ± 0.34	-2.51 ± 0.34	2.21 ± 0.15	0.744
031	NGC4157	0.99 ± 0.12	1.01 ± 0.04	0.53 ± 0.08	0.66 ± 0.14	2.17 ± 0.12	1.02 ± 0.12	1.28 ± 0.23	-2.16 ± 0.29	2.12 ± 0.10	0.448
032	UGC03546	0.87 ± 0.15	0.98 ± 0.08	0.56 ± 0.11	0.59 ± 0.11	2.04 ± 0.03	1.40 ± 0.08	0.78 ± 0.09	-1.21 ± 0.20	2.57 ± 0.11	0.712
033	UGC06787	2.24 ± 0.25	1.07 ± 0.04	0.89 ± 0.12	0.19 ± 0.03	2.44 ± 0.02	0.65 ± 0.05	1.92 ± 0.06	-3.02 ± 0.11	1.90 ± 0.06	17.972
034	NGC4051	0.96 ± 0.13	0.99 ± 0.06	0.46 ± 0.11	.....	1.80 ± 0.26	1.46 ± 0.33	0.47 ± 0.54	-1.03 ± 0.81	2.44 ± 0.37	2.451
035	NGC4217	0.55 ± 0.14	1.00 ± 0.02	0.54 ± 0.13	0.32 ± 0.07	1.96 ± 0.03	1.69 ± 0.12	0.40 ± 0.15	-0.42 ± 0.31	2.98 ± 0.16	1.493
036	NGC3521	1.08 ± 0.19	1.00 ± 0.07	0.54 ± 0.10	.....	2.20 ± 0.14	1.16 ± 0.09	1.18 ± 0.21	-1.83 ± 0.23	2.35 ± 0.10	0.203
037	NGC2903	0.80 ± 0.17	0.99 ± 0.05	0.46 ± 0.12	.....	1.98 ± 0.03	1.58 ± 0.13	0.54 ± 0.16	-0.72 ± 0.36	2.82 ± 0.20	7.458

Table A-1: Continued

SPARC ID	Galaxy Name	$\delta_d$	$\delta_i$	$\Upsilon_d$	$\Upsilon_b$	$\log_{10} V_{200}$ ( $\text{km s}^{-2}$ )	$\log_{10} C_{200}$	$\log_{10} r_0$ (kpc)	$\log_{10} \rho_0$ ( $M_\odot \text{ pc}^{-3}$ )	$\log_{10} \rho_0 r_0$ ( $M_\odot \text{ pc}^{-2}$ )	$\chi^2_v$
038	NGC2683	1.00 ± 0.05	0.99 ± 0.06	0.49 ± 0.10	0.73 ± 0.16	1.96 ± 0.02	1.51 ± 0.12	0.58 ± 0.13	-0.91 ± 0.32	2.67 ± 0.19	1.245
039	NGC4013	1.09 ± 0.11	1.00 ± 0.01	0.57 ± 0.08	0.82 ± 0.18	2.21 ± 0.04	0.93 ± 0.05	1.41 ± 0.08	-2.38 ± 0.12	2.03 ± 0.05	0.836
040	NGC7814	1.00 ± 0.04	1.00 ± 0.01	0.54 ± 0.13	0.62 ± 0.05	2.06 ± 0.01	1.47 ± 0.05	0.73 ± 0.06	-1.03 ± 0.12	2.71 ± 0.06	0.867
041	UGC06786	1.22 ± 0.16	1.02 ± 0.04	0.66 ± 0.09	0.72 ± 0.10	2.17 ± 0.02	1.23 ± 0.07	1.07 ± 0.08	-1.65 ± 0.17	2.43 ± 0.09	2.269
042	NGC3877	0.76 ± 0.14	1.00 ± 0.01	0.30 ± 0.06	.....	1.89 ± 0.02	1.68 ± 0.07	0.35 ± 0.09	-0.46 ± 0.20	2.88 ± 0.11	2.727
043	NGC0289	1.27 ± 0.19	1.10 ± 0.09	0.55 ± 0.09	.....	2.06 ± 0.03	0.90 ± 0.09	1.30 ± 0.09	-2.46 ± 0.21	1.84 ± 0.12	2.144
044	NGC1090	0.65 ± 0.21	1.00 ± 0.05	0.35 ± 0.09	.....	1.95 ± 0.04	1.60 ± 0.15	0.48 ± 0.19	-0.66 ± 0.41	2.82 ± 0.22	1.478
045	NGC3726	1.06 ± 0.12	1.00 ± 0.04	0.61 ± 0.08	.....	2.31 ± 0.18	0.80 ± 0.11	1.64 ± 0.28	-2.69 ± 0.25	1.96 ± 0.12	2.935
046	UGC09037	0.87 ± 0.10	0.93 ± 0.08	0.30 ± 0.05	.....	2.03 ± 0.03	1.25 ± 0.07	0.92 ± 0.08	-1.59 ± 0.17	2.33 ± 0.10	1.091
047	NGC6946	0.92 ± 0.17	0.99 ± 0.05	0.60 ± 0.09	0.64 ± 0.12	1.96 ± 0.04	1.28 ± 0.12	0.81 ± 0.16	-1.50 ± 0.32	2.31 ± 0.16	1.526
048	NGC4100	0.96 ± 0.13	1.00 ± 0.03	0.43 ± 0.07	.....	1.96 ± 0.02	1.58 ± 0.07	0.51 ± 0.08	-0.73 ± 0.19	2.79 ± 0.11	0.631
049	NGC3893	0.97 ± 0.13	0.99 ± 0.04	0.45 ± 0.08	.....	1.97 ± 0.03	1.51 ± 0.11	0.60 ± 0.14	-0.92 ± 0.29	2.68 ± 0.16	0.382
050	UGC06973	0.60 ± 0.11	0.98 ± 0.04	0.31 ± 0.06	0.61 ± 0.13	1.95 ± 0.05	1.70 ± 0.09	0.38 ± 0.14	-0.40 ± 0.24	2.98 ± 0.11	1.622
051	ESO079-G014	0.81 ± 0.21	1.00 ± 0.06	0.46 ± 0.10	.....	2.05 ± 0.02	1.38 ± 0.11	0.80 ± 0.12	-1.24 ± 0.28	2.56 ± 0.15	1.267
052	UGC08699	1.15 ± 0.15	1.03 ± 0.10	0.86 ± 0.14	0.57 ± 0.08	2.07 ± 0.05	1.13 ± 0.08	1.08 ± 0.12	-1.90 ± 0.20	2.17 ± 0.09	0.962
053	NGC4138	0.99 ± 0.13	0.98 ± 0.06	0.50 ± 0.12	0.66 ± 0.15	1.87 ± 0.09	1.65 ± 0.21	0.35 ± 0.29	-0.53 ± 0.56	2.82 ± 0.29	3.291
054	NGC3198	1.06 ± 0.09	1.00 ± 0.04	0.66 ± 0.07	.....	2.01 ± 0.01	1.15 ± 0.04	1.00 ± 0.05	-1.85 ± 0.11	2.15 ± 0.06	1.515
055	NGC3949	1.00 ± 0.12	1.00 ± 0.04	0.53 ± 0.08	.....	2.67 ± 0.29	1.18 ± 0.16	1.62 ± 0.42	-1.76 ± 0.41	2.86 ± 0.23	1.685
056	NGC6015	1.62 ± 0.26	1.01 ± 0.04	0.66 ± 0.15	.....	2.17 ± 0.03	0.73 ± 0.09	1.58 ± 0.11	-2.86 ± 0.21	1.73 ± 0.10	9.552
057	NGC3917	0.95 ± 0.14	1.00 ± 0.03	0.44 ± 0.10	.....	1.91 ± 0.02	1.40 ± 0.07	0.65 ± 0.07	-1.21 ± 0.17	2.44 ± 0.10	1.424
058	NGC4085	0.86 ± 0.13	1.00 ± 0.02	0.35 ± 0.07	.....	1.92 ± 0.24	1.45 ± 0.13	0.61 ± 0.35	-1.06 ± 0.34	2.55 ± 0.15	10.633
059	NGC4389	0.76 ± 0.14	0.90 ± 0.08	0.29 ± 0.06	.....	2.69 ± 0.20	1.28 ± 0.10	1.55 ± 0.23	-1.52 ± 0.25	3.03 ± 0.22	...
060	NGC4559	1.02 ± 0.21	1.00 ± 0.01	0.53 ± 0.10	.....	1.91 ± 0.03	1.15 ± 0.12	0.90 ± 0.14	-1.85 ± 0.29	2.05 ± 0.15	0.266
061	NGC3769	0.97 ± 0.13	1.00 ± 0.03	0.45 ± 0.08	.....	1.90 ± 0.03	1.28 ± 0.09	0.76 ± 0.11	-1.51 ± 0.23	2.25 ± 0.12	0.892
062	NGC4010	0.97 ± 0.14	1.00 ± 0.01	0.45 ± 0.10	.....	1.93 ± 0.12	1.28 ± 0.11	0.79 ± 0.21	-1.52 ± 0.27	2.27 ± 0.11	2.311
063	NGC3972	0.97 ± 0.14	1.00 ± 0.01	0.44 ± 0.12	.....	1.87 ± 0.09	1.45 ± 0.11	0.56 ± 0.18	-1.08 ± 0.27	2.48 ± 0.12	1.384
064	UGC03580	0.59 ± 0.11	0.98 ± 0.06	1.10 ± 0.18	0.29 ± 0.05	1.93 ± 0.03	1.32 ± 0.06	0.75 ± 0.08	-1.42 ± 0.15	2.33 ± 0.07	2.680
065	NGC6503	0.99 ± 0.05	1.00 ± 0.03	0.57 ± 0.04	.....	1.87 ± 0.01	1.31 ± 0.02	0.69 ± 0.03	-1.43 ± 0.06	2.26 ± 0.03	2.631
066	UGC11557	0.92 ± 0.26	0.66 ± 0.29	0.46 ± 0.11	.....	1.93 ± 0.25	1.34 ± 0.34	0.72 ± 0.47	-1.37 ± 0.87	2.36 ± 0.53	0.771
067	UGC00128	0.99 ± 0.15	1.03 ± 0.14	0.32 ± 0.08	.....	1.96 ± 0.04	1.20 ± 0.05	0.90 ± 0.06	-1.73 ± 0.14	2.18 ± 0.10	9.834
068	F579-V1	1.00 ± 0.10	1.37 ± 0.40	0.50 ± 0.15	.....	1.59 ± 0.25	1.60 ± 0.30	0.12 ± 0.46	-0.67 ± 0.71	2.46 ± 0.40	0.197
069	NGC4183	0.96 ± 0.15	1.00 ± 0.02	0.48 ± 0.22	.....	1.80 ± 0.14	1.42 ± 0.20	0.52 ± 0.33	-1.14 ± 0.48	2.38 ± 0.18	0.464
070	F571-8	0.47 ± 0.14	0.99 ± 0.05	0.36 ± 0.09	.....	1.94 ± 0.04	1.59 ± 0.10	0.48 ± 0.14	-0.69 ± 0.28	2.79 ± 0.14	0.562
071	NGC2403	0.94 ± 0.05	0.93 ± 0.05	0.90 ± 0.07	.....	1.93 ± 0.01	1.32 ± 0.02	0.74 ± 0.02	-1.40 ± 0.05	2.34 ± 0.04	11.803
072	UGC06930	1.00 ± 0.14	1.00 ± 0.17	0.49 ± 0.14	.....	1.79 ± 0.10	1.37 ± 0.15	0.56 ± 0.17	-1.27 ± 0.37	2.29 ± 0.25	0.354
073	F568-3	1.00 ± 0.10	0.83 ± 0.23	0.48 ± 0.11	.....	1.96 ± 0.11	1.28 ± 0.12	0.82 ± 0.07	-1.51 ± 0.32	2.31 ± 0.29	1.289
074	UGC01230	0.98 ± 0.20	0.85 ± 0.38	0.49 ± 0.12	.....	1.90 ± 0.22	1.44 ± 0.21	0.60 ± 0.12	-1.10 ± 0.56	2.50 ± 0.54	0.434
075	NGC0247	1.06 ± 0.05	1.03 ± 0.04	2.12 ± 0.60	.....	2.66 ± 0.42	0.60 ± 0.34	2.19 ± 0.75	-3.13 ± 0.81	2.06 ± 0.18	2.178
076	NGC7793	1.01 ± 0.05	1.18 ± 0.14	0.58 ± 0.09	.....	1.67 ± 0.23	1.28 ± 0.14	0.53 ± 0.35	-1.51 ± 0.36	2.01 ± 0.16	0.784

Table A-1: Continued

SPARC ID	Galaxy Name	$\delta_d$	$\delta_i$	$\Upsilon_d$	$\Upsilon_b$	$\log_{10} V_{200}$ ( $\text{km s}^{-2}$ )	$\log_{10} C_{200}$	$\log_{10} r_0$ (kpc)	$\log_{10} \rho_0$ ( $M_\odot \text{pc}^{-3}$ )	$\log_{10} \rho_0 r_0$ ( $M_\odot \text{pc}^{-2}$ )	$\chi^2_v$
077	UGC06917	0.99 ± 0.14	0.99 ± 0.04	0.49 ± 0.11	.....	1.81 ± 0.03	1.39 ± 0.07	0.55 ± 0.09	-1.23 ± 0.19	2.33 ± 0.10	0.346
078	NGC1003	1.29 ± 0.20	1.03 ± 0.07	0.74 ± 0.12	.....	1.98 ± 0.02	0.86 ± 0.07	1.26 ± 0.08	-2.55 ± 0.17	1.70 ± 0.09	3.117
079	F574-1	0.99 ± 0.10	0.98 ± 0.16	0.49 ± 0.12	.....	1.79 ± 0.04	1.39 ± 0.06	0.54 ± 0.06	-1.23 ± 0.16	2.31 ± 0.12	0.134
080	F568-1	0.99 ± 0.11	0.99 ± 0.20	0.49 ± 0.12	.....	1.91 ± 0.09	1.46 ± 0.09	0.59 ± 0.08	-1.05 ± 0.24	2.54 ± 0.21	0.149
081	UGC06983	1.01 ± 0.14	1.00 ± 0.02	0.51 ± 0.12	.....	1.80 ± 0.02	1.43 ± 0.07	0.51 ± 0.08	-1.12 ± 0.18	2.39 ± 0.10	0.575
082	UGC05986	1.08 ± 0.26	1.00 ± 0.02	0.50 ± 0.11	.....	1.85 ± 0.03	1.43 ± 0.11	0.56 ± 0.14	-1.13 ± 0.29	2.43 ± 0.15	1.244
083	NGC0055	0.99 ± 0.05	1.00 ± 0.04	0.39 ± 0.07	.....	1.81 ± 0.02	1.14 ± 0.03	0.80 ± 0.04	-1.86 ± 0.08	1.94 ± 0.04	0.415
084	ESO116-G012	1.06 ± 0.25	1.00 ± 0.04	0.53 ± 0.11	.....	1.84 ± 0.03	1.37 ± 0.11	0.60 ± 0.14	-1.27 ± 0.30	2.33 ± 0.16	1.090
085	UGC07323	1.08 ± 0.27	1.01 ± 0.06	0.51 ± 0.12	.....	1.81 ± 0.32	1.19 ± 0.18	0.76 ± 0.46	-1.75 ± 0.45	2.01 ± 0.25	0.518
086	UGC05005	1.02 ± 0.21	0.98 ± 0.26	0.49 ± 0.12	.....	1.91 ± 0.15	1.01 ± 0.23	1.03 ± 0.31	-2.19 ± 0.54	1.84 ± 0.31	0.024
087	F561-1	1.00 ± 0.15	0.79 ± 0.32	0.48 ± 0.12	.....	1.54 ± 0.36	1.29 ± 0.38	0.39 ± 0.59	-1.49 ± 0.93	1.90 ± 0.59	...
088	NGC0024	0.99 ± 0.06	0.99 ± 0.06	0.44 ± 0.65	.....	1.75 ± 0.24	1.71 ± 0.34	0.18 ± 0.56	-0.38 ± 0.87	2.80 ± 0.35	0.893
089	F568-V1	1.00 ± 0.10	1.01 ± 0.27	0.49 ± 0.12	.....	1.83 ± 0.11	1.50 ± 0.12	0.47 ± 0.08	-0.94 ± 0.31	2.53 ± 0.28	0.079
090	UGC06628	0.97 ± 0.29	0.75 ± 0.30	0.49 ± 0.12	.....	1.41 ± 0.43	1.53 ± 0.51	0.01 ± 0.85	-0.85 ± 1.24	2.16 ± 0.60	0.246
091	UGC02455	0.19 ± 0.10	0.98 ± 0.10	0.46 ± 0.11	.....	2.68 ± 0.23	1.65 ± 0.14	1.16 ± 0.29	-0.53 ± 0.39	3.63 ± 0.31	1.647
092	UGC07089	1.01 ± 0.14	0.99 ± 0.04	0.51 ± 0.14	.....	1.78 ± 0.31	1.10 ± 0.13	0.81 ± 0.43	-1.96 ± 0.33	1.85 ± 0.20	0.252
093	UGC05999	0.96 ± 0.21	0.79 ± 0.35	0.49 ± 0.12	.....	1.95 ± 0.24	1.24 ± 0.24	0.85 ± 0.26	-1.61 ± 0.63	2.24 ± 0.54	...
094	NGC2976	0.99 ± 0.05	1.00 ± 0.14	0.49 ± 0.10	.....	1.83 ± 0.30	1.45 ± 0.10	0.51 ± 0.37	-1.06 ± 0.26	2.46 ± 0.26	0.361
095	UGC05750	0.98 ± 0.21	1.00 ± 0.17	0.49 ± 0.13	.....	1.79 ± 0.12	1.06 ± 0.14	0.87 ± 0.21	-2.07 ± 0.34	1.80 ± 0.21	0.210
096	NGC0100	0.98 ± 0.29	1.00 ± 0.01	0.49 ± 0.11	.....	1.80 ± 0.09	1.27 ± 0.17	0.66 ± 0.24	-1.53 ± 0.43	2.13 ± 0.20	0.107
097	UGC00634	0.99 ± 0.25	1.03 ± 0.22	0.49 ± 0.12	.....	1.89 ± 0.08	1.19 ± 0.16	0.84 ± 0.15	-1.75 ± 0.40	2.08 ± 0.28	...
098	F563-V2	1.00 ± 0.20	0.95 ± 0.34	0.52 ± 0.12	.....	1.85 ± 0.16	1.54 ± 0.16	0.45 ± 0.12	-0.83 ± 0.43	2.62 ± 0.40	0.353
099	NGC5585	1.15 ± 0.20	1.00 ± 0.04	0.53 ± 0.10	.....	1.82 ± 0.02	1.18 ± 0.06	0.78 ± 0.07	-1.78 ± 0.16	2.00 ± 0.09	5.256
100	NGC0300	1.01 ± 0.05	1.11 ± 0.23	0.56 ± 0.14	.....	1.76 ± 0.07	1.28 ± 0.12	0.62 ± 0.12	-1.51 ± 0.32	2.11 ± 0.23	0.656
101	UGC06923	1.00 ± 0.14	1.00 ± 0.03	0.47 ± 0.12	.....	1.73 ± 0.28	1.34 ± 0.14	0.52 ± 0.41	-1.35 ± 0.36	2.17 ± 0.18	...
102	F574-2	0.99 ± 0.10	0.96 ± 0.24	0.51 ± 0.12	.....	1.30 ± 0.53	0.63 ± 0.46	0.81 ± 0.88	-3.07 ± 1.06	0.74 ± 0.50	...
103	UGC07125	0.84 ± 0.21	1.00 ± 0.02	0.50 ± 0.12	.....	1.62 ± 0.02	1.15 ± 0.12	0.61 ± 0.12	-1.84 ± 0.29	1.77 ± 0.17	0.290
104	UGC07524	1.00 ± 0.05	1.01 ± 0.06	0.54 ± 0.12	.....	1.70 ± 0.03	1.28 ± 0.03	0.56 ± 0.03	-1.52 ± 0.08	2.04 ± 0.07	0.260
105	UGC06399	0.99 ± 0.14	1.00 ± 0.03	0.50 ± 0.12	.....	1.75 ± 0.04	1.35 ± 0.07	0.54 ± 0.10	-1.33 ± 0.19	2.21 ± 0.09	0.110
106	UGC07151	1.00 ± 0.05	1.00 ± 0.02	0.52 ± 0.22	.....	1.57 ± 0.21	1.51 ± 0.14	0.20 ± 0.34	-0.92 ± 0.36	2.28 ± 0.09	1.627
107	F567-2	1.01 ± 0.15	0.93 ± 0.46	0.49 ± 0.13	.....	1.54 ± 0.36	1.27 ± 0.39	0.40 ± 0.55	-1.53 ± 0.94	1.87 ± 0.66	...
108	UGC04325	0.92 ± 0.28	1.00 ± 0.07	0.50 ± 0.12	.....	1.65 ± 0.04	1.69 ± 0.11	0.10 ± 0.13	-0.43 ± 0.30	2.67 ± 0.17	1.192
109	UGC00191	1.13 ± 0.35	1.05 ± 0.13	0.46 ± 0.26	.....	1.64 ± 0.33	1.42 ± 0.44	0.36 ± 0.75	-1.15 ± 1.06	2.21 ± 0.39	9.026
110	F563-1	0.99 ± 0.20	0.97 ± 0.22	0.49 ± 0.12	.....	1.86 ± 0.10	1.39 ± 0.12	0.60 ± 0.11	-1.23 ± 0.31	2.38 ± 0.25	0.765
111	F571-V1	1.00 ± 0.10	1.01 ± 0.37	0.48 ± 0.12	.....	1.78 ± 0.20	1.18 ± 0.24	0.73 ± 0.31	-1.76 ± 0.60	1.97 ± 0.42	0.164
112	UGC07261	0.98 ± 0.30	0.93 ± 0.35	0.49 ± 0.12	.....	1.62 ± 0.29	1.58 ± 0.37	0.18 ± 0.59	-0.74 ± 0.93	2.44 ± 0.47	1.783
113	UGC10310	0.94 ± 0.31	1.00 ± 0.19	0.50 ± 0.14	.....	1.61 ± 0.16	1.44 ± 0.23	0.31 ± 0.33	-1.09 ± 0.56	2.21 ± 0.31	0.445
114	UGC02259	1.02 ± 0.29	1.01 ± 0.08	0.46 ± 0.11	.....	1.66 ± 0.04	1.59 ± 0.11	0.21 ± 0.13	-0.70 ± 0.30	2.51 ± 0.17	6.781
115	F583-4	1.00 ± 0.21	1.04 ± 0.20	0.51 ± 0.16	.....	1.60 ± 0.26	1.32 ± 0.23	0.41 ± 0.45	-1.40 ± 0.57	2.01 ± 0.25	0.740

Table A-1: Continued

SPARC ID	Galaxy Name	$\delta_d$	$\delta_i$	$\Upsilon_d$	$\Upsilon_i$	$\log_{10} V_{200}$ ( $\text{km s}^{-2}$ )	$\log_{10} C_{200}$	$\log_{10} r_0$ (kpc)	$\log_{10} \rho_0 r_0$ ( $M_\odot \text{pc}^{-3}$ )	$\log_{10} \rho_0$ ( $M_\odot \text{pc}^{-2}$ )	$\chi^2_v$
116	UGC12732	1.48 ± 0.27	1.23 ± 0.13	0.53 ± 0.18	.....	1.68 ± 0.10	1.09 ± 0.15	0.73 ± 0.22	-2.00 ± 0.37	1.73 ± 0.20	0.527
117	UGC06818	0.95 ± 0.14	0.99 ± 0.04	0.46 ± 0.09	.....	2.11 ± 0.24	1.08 ± 0.07	1.16 ± 0.28	-2.01 ± 0.17	2.15 ± 0.22	3.257
118	UGC04499	0.92 ± 0.32	1.00 ± 0.06	0.49 ± 0.13	.....	1.65 ± 0.18	1.35 ± 0.21	0.44 ± 0.36	-1.34 ± 0.52	2.10 ± 0.21	0.514
119	F563-V1	1.02 ± 0.18	0.99 ± 0.16	0.51 ± 0.12	.....	1.12 ± 0.60	0.97 ± 0.45	0.28 ± 0.99	-2.28 ± 1.01	1.00 ± 0.41	....
120	UGC06667	1.01 ± 0.14	1.00 ± 0.01	0.49 ± 0.12	.....	1.75 ± 0.02	1.39 ± 0.05	0.50 ± 0.07	-1.23 ± 0.14	2.26 ± 0.07	0.221
121	UGC02023	0.99 ± 0.29	0.88 ± 0.41	0.50 ± 0.12	.....	2.60 ± 0.31	1.14 ± 0.34	1.59 ± 0.45	-1.86 ± 0.84	2.73 ± 0.60	....
122	UGC04278	1.17 ± 0.22	0.99 ± 0.02	0.61 ± 0.15	.....	1.95 ± 0.19	1.15 ± 0.09	0.94 ± 0.25	-1.85 ± 0.23	2.08 ± 0.15	0.629
123	UGC12632	1.07 ± 0.29	1.00 ± 0.07	0.51 ± 0.12	.....	1.65 ± 0.03	1.31 ± 0.12	0.48 ± 0.14	-1.44 ± 0.30	2.04 ± 0.18	0.090
124	UGC08286	1.00 ± 0.03	1.00 ± 0.02	0.42 ± 0.09	.....	1.67 ± 0.01	1.55 ± 0.02	0.25 ± 0.03	-0.79 ± 0.05	2.46 ± 0.03	1.588
125	UGC07399	1.13 ± 0.29	1.01 ± 0.05	0.54 ± 0.13	.....	1.72 ± 0.04	1.61 ± 0.11	0.25 ± 0.14	-0.65 ± 0.30	2.60 ± 0.16	1.614
126	NGC4214	1.01 ± 0.05	1.48 ± 0.22	0.55 ± 0.12	.....	1.61 ± 0.24	1.25 ± 0.16	0.49 ± 0.36	-1.59 ± 0.41	1.90 ± 0.22	1.205
127	UGC05414	1.01 ± 0.32	1.00 ± 0.05	0.49 ± 0.13	.....	1.64 ± 0.36	1.28 ± 0.21	0.49 ± 0.54	-1.52 ± 0.53	1.98 ± 0.24	....
128	UGC08490	1.09 ± 0.11	1.04 ± 0.06	0.81 ± 0.19	.....	1.64 ± 0.02	1.48 ± 0.09	0.30 ± 0.10	-0.98 ± 0.24	2.31 ± 0.14	0.431
129	IC2574	1.03 ± 0.05	1.05 ± 0.08	0.71 ± 0.10	.....	1.95 ± 0.15	0.87 ± 0.04	1.22 ± 0.18	-2.53 ± 0.09	1.69 ± 0.12	2.482
130	UGC06446	1.17 ± 0.29	1.01 ± 0.06	0.50 ± 0.13	.....	1.67 ± 0.03	1.45 ± 0.11	0.35 ± 0.13	-1.07 ± 0.28	2.29 ± 0.16	0.552
131	F583-1	0.91 ± 0.24	0.98 ± 0.08	0.48 ± 0.12	.....	1.77 ± 0.04	1.29 ± 0.10	0.62 ± 0.13	-1.49 ± 0.27	2.13 ± 0.15	0.218
132	UGC11820	1.36 ± 0.23	1.22 ± 0.17	1.38 ± 0.18	.....	1.81 ± 0.27	0.68 ± 0.22	1.26 ± 0.47	-2.96 ± 0.47	1.30 ± 0.18	3.192
133	UGC07690	0.99 ± 0.29	1.00 ± 0.13	0.50 ± 0.13	.....	1.41 ± 0.28	1.70 ± 0.32	-0.15 ± 0.57	-0.40 ± 0.83	2.45 ± 0.35	0.573
134	UGC04305	1.00 ± 0.05	0.55 ± 0.19	0.52 ± 0.18	.....	1.47 ± 0.32	1.58 ± 0.45	0.02 ± 0.72	-0.71 ± 1.04	2.31 ± 0.44	1.142
135	NGC2915	0.99 ± 0.05	0.97 ± 0.07	0.42 ± 0.09	.....	1.70 ± 0.02	1.53 ± 0.05	0.31 ± 0.06	-0.85 ± 0.12	2.46 ± 0.07	0.577
136	UGC05716	1.45 ± 0.20	1.26 ± 0.14	0.76 ± 0.17	.....	1.64 ± 0.03	1.05 ± 0.07	0.72 ± 0.07	-2.10 ± 0.18	1.62 ± 0.12	2.695
137	UGC05829	1.06 ± 0.31	1.10 ± 0.32	0.49 ± 0.15	.....	1.56 ± 0.28	1.20 ± 0.22	0.50 ± 0.40	-1.72 ± 0.54	1.77 ± 0.40	0.327
138	F565-V2	0.99 ± 0.20	0.99 ± 0.17	0.49 ± 0.12	.....	1.82 ± 0.17	1.22 ± 0.13	0.74 ± 0.26	-1.68 ± 0.32	2.06 ± 0.18	0.308
139	DDO161	1.02 ± 0.22	1.01 ± 0.12	0.50 ± 0.10	.....	1.74 ± 0.04	0.99 ± 0.11	0.88 ± 0.14	-2.23 ± 0.28	1.65 ± 0.14	0.305
140	DDO170	0.70 ± 0.26	0.98 ± 0.11	0.48 ± 0.12	.....	1.62 ± 0.04	1.30 ± 0.14	0.45 ± 0.17	-1.46 ± 0.36	1.99 ± 0.20	3.953
141	NGC1705	1.00 ± 0.05	1.02 ± 0.10	0.56 ± 0.14	.....	1.53 ± 0.03	1.78 ± 0.07	-0.11 ± 0.09	-0.19 ± 0.20	2.71 ± 0.11	0.925
142	UGC05721	1.08 ± 0.26	1.01 ± 0.08	0.52 ± 0.12	.....	1.61 ± 0.03	1.69 ± 0.11	0.05 ± 0.13	-0.42 ± 0.28	2.63 ± 0.16	0.467
143	UGC08837	1.00 ± 0.05	1.00 ± 0.06	0.47 ± 0.09	.....	2.61 ± 0.25	0.98 ± 0.04	1.77 ± 0.27	-2.26 ± 0.09	2.50 ± 0.24	1.007
144	UGC07603	0.97 ± 0.29	1.00 ± 0.04	0.48 ± 0.11	.....	1.56 ± 0.05	1.54 ± 0.14	0.16 ± 0.18	-0.84 ± 0.37	2.32 ± 0.19	0.328
145	UGC00891	0.95 ± 0.29	1.00 ± 0.09	0.49 ± 0.12	.....	1.73 ± 0.05	1.16 ± 0.15	0.70 ± 0.20	-1.81 ± 0.37	1.89 ± 0.18	....
146	UGC01281	0.98 ± 0.04	1.00 ± 0.01	0.50 ± 0.12	.....	1.62 ± 0.04	1.29 ± 0.03	0.47 ± 0.07	-1.49 ± 0.09	1.99 ± 0.04	0.347
147	UGC09992	1.00 ± 0.27	0.99 ± 0.31	0.48 ± 0.13	.....	1.18 ± 0.58	1.59 ± 0.61	-0.27 ± 1.14	-0.71 ± 1.47	2.03 ± 0.52	....
148	D512-2	1.03 ± 0.32	1.03 ± 0.19	0.51 ± 0.14	.....	1.37 ± 0.33	1.33 ± 0.23	0.18 ± 0.51	-1.39 ± 0.60	1.79 ± 0.30	....
149	UGC00731	1.25 ± 0.26	1.01 ± 0.05	0.52 ± 0.12	.....	1.64 ± 0.02	1.33 ± 0.07	0.45 ± 0.08	-1.39 ± 0.18	2.06 ± 0.11	0.658
150	UGC08550	1.18 ± 0.28	1.00 ± 0.02	0.51 ± 0.15	.....	1.51 ± 0.04	1.45 ± 0.12	0.20 ± 0.16	-1.06 ± 0.32	2.14 ± 0.17	1.548
151	UGC07608	1.00 ± 0.29	0.96 ± 0.40	0.49 ± 0.12	.....	1.71 ± 0.28	1.36 ± 0.23	0.48 ± 0.36	-1.30 ± 0.60	2.18 ± 0.47	0.240
152	NGC4068	1.00 ± 0.05	0.99 ± 0.14	0.49 ± 0.11	.....	2.47 ± 0.35	1.12 ± 0.10	1.49 ± 0.39	-1.91 ± 0.24	2.57 ± 0.32	....
153	NGC2366	1.00 ± 0.05	0.99 ± 0.07	0.38 ± 0.07	.....	1.54 ± 0.02	1.29 ± 0.03	0.39 ± 0.04	-1.49 ± 0.09	1.90 ± 0.06	0.908
154	UGC05918	0.99 ± 0.31	1.00 ± 0.11	0.51 ± 0.12	.....	1.42 ± 0.07	1.40 ± 0.14	0.15 ± 0.18	-1.20 ± 0.37	1.95 ± 0.21	0.141

Table A-1: Continued

SPARC ID	Galaxy Name	$\delta_d$	$\delta_i$	$\Upsilon_d$	$\Upsilon_b$	$\log_{10} V_{200}$ ( $\text{km s}^{-2}$ )	$\log_{10} C_{200}$	$\log_{10} r_0$ (kpc)	$\log_{10} \rho_0$ ( $\text{M}_\odot \text{pc}^{-3}$ )	$\log_{10} \rho_0 r_0$ ( $\text{M}_\odot \text{pc}^{-2}$ )	$\chi^2_\nu$
155	D631-7	0.99 ± 0.02	0.96 ± 0.05	0.39 ± 0.08	.....	1.80 ± 0.08	1.11 ± 0.03	0.83 ± 0.10	-1.94 ± 0.08	1.89 ± 0.06	1.001
156	NGC3109	1.00 ± 0.05	1.00 ± 0.07	0.50 ± 0.12	.....	1.75 ± 0.02	1.22 ± 0.03	0.67 ± 0.04	-1.67 ± 0.07	2.00 ± 0.04	0.214
157	UGCA281	1.00 ± 0.05	1.00 ± 0.04	0.50 ± 0.17	.....	1.20 ± 0.31	1.58 ± 0.10	-0.25 ± 0.39	-0.72 ± 0.25	2.03 ± 0.20	0.570
158	DDO168	0.97 ± 0.05	0.87 ± 0.09	0.46 ± 0.10	.....	1.71 ± 0.04	1.32 ± 0.04	0.53 ± 0.07	-1.41 ± 0.12	2.12 ± 0.08	7.568
159	DDO064	1.04 ± 0.30	1.02 ± 0.08	0.49 ± 0.13	.....	1.52 ± 0.32	1.37 ± 0.15	0.28 ± 0.42	-1.27 ± 0.39	2.01 ± 0.28	0.509
160	PGC51017	1.02 ± 0.09	1.01 ± 0.04	0.56 ± 0.10	.....	2.61 ± 0.41	0.00 ± 0.20	2.75 ± 0.51	-4.11 ± 0.37	1.64 ± 0.39	...
161	UGCA442	0.99 ± 0.05	1.00 ± 0.11	0.50 ± 0.12	.....	1.60 ± 0.03	1.29 ± 0.05	0.45 ± 0.05	-1.49 ± 0.12	1.96 ± 0.08	1.867
162	UGC07866	1.00 ± 0.05	1.00 ± 0.12	0.48 ± 0.14	.....	1.25 ± 0.55	1.39 ± 0.18	-0.01 ± 0.70	-1.23 ± 0.46	1.77 ± 0.37	0.348
163	UGC07232	1.00 ± 0.06	1.00 ± 0.08	0.50 ± 0.11	.....	2.49 ± 0.32	1.51 ± 0.05	1.11 ± 0.34	-0.90 ± 0.14	3.21 ± 0.30	...
164	UGC07559	0.99 ± 0.05	0.99 ± 0.05	0.49 ± 0.13	.....	1.39 ± 0.45	1.22 ± 0.09	0.31 ± 0.52	-1.66 ± 0.22	1.65 ± 0.37	0.521
165	NGC6789	0.99 ± 0.05	1.01 ± 0.16	0.50 ± 0.12	.....	1.75 ± 0.34	1.75 ± 0.07	0.13 ± 0.37	-0.27 ± 0.19	2.87 ± 0.32	...
166	KK98-251	1.12 ± 0.32	1.03 ± 0.09	0.48 ± 0.13	.....	1.52 ± 0.43	1.06 ± 0.20	0.60 ± 0.58	-2.07 ± 0.48	1.52 ± 0.32	0.398
167	UGC05764	0.97 ± 0.26	1.00 ± 0.16	0.48 ± 0.12	.....	1.47 ± 0.05	1.62 ± 0.09	-0.02 ± 0.11	-0.62 ± 0.24	2.36 ± 0.15	5.065
168	CamB	0.91 ± 0.08	0.90 ± 0.08	0.34 ± 0.07	.....	2.67 ± 0.27	0.97 ± 0.06	1.84 ± 0.28	-2.29 ± 0.15	2.55 ± 0.28	4.135
169	ESO444-G084	1.01 ± 0.10	1.04 ± 0.22	0.55 ± 0.14	.....	1.57 ± 0.08	1.50 ± 0.13	0.20 ± 0.15	-0.94 ± 0.33	2.27 ± 0.22	7.899
170	DDO154	1.00 ± 0.05	1.00 ± 0.05	0.43 ± 0.08	.....	1.54 ± 0.01	1.26 ± 0.02	0.42 ± 0.03	-1.56 ± 0.06	1.86 ± 0.04	1.896
171	UGC07577	1.00 ± 0.05	1.00 ± 0.05	0.49 ± 0.11	.....	2.51 ± 0.37	0.82 ± 0.20	1.83 ± 0.44	-2.65 ± 0.42	2.18 ± 0.41	0.296
172	D564-8	1.00 ± 0.03	1.00 ± 0.11	0.51 ± 0.13	.....	1.33 ± 0.34	1.14 ± 0.09	0.33 ± 0.41	-1.87 ± 0.22	1.46 ± 0.25	...
173	NGC3741	1.03 ± 0.05	1.03 ± 0.05	0.77 ± 0.17	.....	1.56 ± 0.02	1.23 ± 0.03	0.47 ± 0.04	-1.65 ± 0.08	1.82 ± 0.04	0.988
174	UGC04483	0.99 ± 0.10	1.00 ± 0.05	0.49 ± 0.15	.....	1.11 ± 0.33	1.52 ± 0.12	-0.27 ± 0.44	-0.89 ± 0.32	1.84 ± 0.20	0.744
175	UGCA444	1.00 ± 0.05	0.99 ± 0.05	0.51 ± 0.12	.....	1.33 ± 0.05	1.38 ± 0.04	0.09 ± 0.09	-1.25 ± 0.12	1.83 ± 0.05	0.245